EPRI

Tube Repair and Protection for Damage Caused by Sootblower Erosion

Technical Report

Tube Repair and Protection for Damage Caused by Sootblower Erosion

1008037

Final Report, March 2004

EPRI Project Managers
K. Coleman
D. Overcash

EPRI • 3412 Hillview Avenue, Palo Alto, California 94304 • PO Box 10412, Palo Alto, California 94303 • USA
800.313.3774 • 650.855.2121 • askepri@epri.com • www.epri.com

DISCLAIMER OF WARRANTIES AND LIMITATION OF LIABILITIES

ORGANIZATION(S) THAT PREPARED THIS DOCUMENT

EPRI

ORDERING INFORMATION

Requests for copies of this report should be directed to EPRI Orders and Conferences, 1355 Willow Way, Suite 278, Concord, CA 94520, (800) 313-3774, press 2 or internally x5379, (925) 609-9169, (925) 609-1310 (fax).

CITATIONS

This report was prepared by

Fossil Repair Applications Center (FRAC)
EPRI
1300 W.T. Harris Boulevard
Charlotte, NC 28262

Principal Investigators
K. Coleman
D. Overcash

This report describes research sponsored by EPRI.

The report is a corporate document that should be cited in the literature in the following manner:

Tube Repair and Protection for Damage Caused by Sootblower Erosion, EPRI, Palo Alto, CA: 2004. 1008037.

REPORT SUMMARY

This report provides several key essentials in solving the problems associated with fireside tube wastage in boiler units caused partly by the use of sootblowers. The report includes: relevant background information, discussion of wear and erosion, repair techniques, discussion of intensively researched high-temperature erosion-resistant alloys, testing results, and optimum alloys for overlaying waterwall and superheat/reheat (SH/RH) tubing from a performance perspective.

Background

Tubes in boiler units begin to develop fouling in the form of soot buildup over time as a result of the combustion of coal. Fouling is characterized as an additional layer of low thermal conductivity material that adheres to another material's surface, thus creating a large temperature drop across the undesired fouling thickness. Because a large temperature drop exists, a greater amount of energy must be supplied to perform the same change of state conditions (that is, the conversion of subcooled water to steam in waterwall tubes). Therefore, the efficiency of the boiler greatly diminishes. To reestablish the optimum heat transfer capabilities, sootblowers must be used to clean tube surfaces on an as-needed basis. There is also an issue of sootblowing too often, which can remove the protective oxide layer from the boiler tubing, thus exposing a surface favoring corrosion. It is still unclear whether the wastage of tubes is caused by direct erosion from sootblowers or due to an enhanced mechanism known as erosion-corrosion that occurs from a mixture of sootblowing too often and a corrosive boiler environment.

Objectives

- To provide the user of this document with relevant background information
- To discuss the theoretical and physical aspects of tube wastage
- To test selected tube overlays for high-temperature erosion resistance
- To discuss how in-service tube wastage can be limited by applying the optimal alloy, evaluated on the basis of cost, boiler environment, ease of application, and performance

Approach

A list of twelve alloys was generated through extensive research on high-temperature erosion resistance. Eleven coupons were prepared by depositing these alloys on SA387 Gr. 11 base metal, and one coupon was prepared from the base metal itself. Four permutations of high-temperature erosion tests were performed which included: 1) 30º impact, 900ºF (482ºC); 2) 90º impact, 900ºF (482ºC); 3) 30º impact, 1100ºF (593ºC); 4) 90º impact, 1100ºF (593ºC). Performance comparisons were given to support the user in identifying optimum alloys for both waterwall and SH/RH environments.

Results

The results indicate that the high-velocity oxy-fuel (HVOF)-sprayed Cr_3C_2-NiCr coating and infiltration brazed WC200 alloy exhibited the lowest thickness losses through all permutations of high-temperature erosion testing. The HVOF-applied LMC-M tungsten carbide blend consistently showed the third-lowest erosion wastage, except at the conditions of 90° impact 1100 °F (593ºC). The nickel alloys and stainless steels followed, with the stainless steels more erosion-resistant at the higher of the testing temperatures and the nickel alloys more erosion-resistant at the lower of the testing temperatures. The SA387 Gr.11 alloy steel base metal and Duocor coating consistently showed the highest erosion wastage, with the Duocor coating actually wearing through the applied thickness at normal impacts to the tube surface**.**

EPRI Perspective

EPRI's intention in issuing the results of high-temperature erosion testing is not to indicate that one alloy outperforms another on a consistent basis. Rather, EPRI tested these alloys for informational purposes only. This information can be used by utilities as a guide in the selection process for defining optimum alloys for a given environment. In selecting an optimal alloy, other issues such as cost, suitability in a given boiler environment, and ease of application should also be taken into consideration. Several of the alloys cannot be applied in the field and are more suitable to replacement than repair.

Keywords

Boiler
Erosion-corrosion
Fouling
Sootblower
Superheat/reheat
Tube wastage

ACKNOWLEDGMENTS

The authors of this report would like to thank several key people who contributed to the research, material availability, and testing used to produce this document:

High-temperature erosion testing:

Dr. Buqian Wang Zheng Rong Shui (Wang's Consultant)

Thermal coating and weld overlay vendors**:**

Larry Robbins	Liquidmetal Coatings
Scott Trunkett	Conforma Clad
Gregg Clark	ThyssenKrupp VDM USA, Inc.
Iain Hall	Metalspray

ABSTRACT

Fireside tube wastage in fossil power plant boilers has become a major problem for utilities. The cause of wastage is still unclear—it may be strictly by erosion through the direct utilization of sootblowers or by erosion-corrosion through a combination of sootblowers and the environment. Primary investigation in this report focuses on the effect of high-temperature erosion. Material aging, thermal fatigue, and corrosion may also play important roles in the overall wastage. This brings forth the need to identify optimum alloys for protection against tube damage.

This report covers several areas important in sootblower erosion repair. First, the report establishes an appropriate background for the user, concentrating on sootblower types, cleaning media, and damage mechanisms. Wear and erosion are addressed in a more technical discussion, which incorporates erosion testing methods, mathematical erosion models, and high-temperature material wear data. Discussion of thoroughly researched high-temperature erosion-resistant alloys is provided and test results are compared. Optimum alloys for waterwall and superheat/reheat (SH/RH) environments are then determined from a performance standpoint. Repair methods are identified for application of optimum alloys, including weld overlays and thermal-spray coatings.

CONTENTS

LIST OF FIGURES

LIST OF TABLES

1
INTRODUCTION

Fireside waterwall and superheat/reheat (SH/RH) tube wastage is a major concern in operating boilers. If excessive tube wastage is not identified in sufficient time, damage may occur in the form of small leaks or massive failures (that is, a tube bursting, requiring the plant to be shut down). The resultant expense is not only a factor of the repair itself, but also incorporates relatively large revenue losses due to boiler unavailability. However, if tube wastage is recognized in a timely manner (for example, a minimum wall thickness is violated), repairs can be performed that will allow the plant to operate without forced outages. Tube wastage is a result of erosion through direct use of sootblowers or due to an enhanced mechanism known as erosion-corrosion, which is developed through erosive sootblowing in a corrosive environment.

Why use sootblowers? Sootblowers must be utilized in boiler units to clean soot buildup on waterwall surfaces and unclog gas passageways in SH/RH tubes. Soot buildup on tube surfaces adds an undesired layer with low thermal conductivity, thus creating a large temperature drop across its thickness. As a result, a greater amount of energy must be supplied to convert the incoming subcooled water in the waterwalls to steam. Regular sootblowing on an as-needed basis removes this extra layer of thermal resistance and creates a more efficient boiler unit by means of enhanced heat transfer across the tube surfaces.

Sootblowing too frequently removes the protective oxide layer from the tubing. This oxide layer is important in resisting the corrosive destruction of tube surfaces in the specific environment. The actual mechanism behind tube wastage still remains unclear—it may be due either to erosion or erosion-corrosion.

Erosion rates vary with several key elements including:

- Impact velocity and angle
- Tube surface temperature, modulus of elasticity, hardness, and erosion resistance
- Erodent hardness and shape
- Environment

These elements are discussed in appropriate detail in the following sections of this report. Many of these elements cannot be varied to reduce erosion and/or erosion-corrosion of tube surfaces. However, one area that can be examined is material high-temperature erosion resistance. It is the purpose of this report to introduce sootblowers, damage mechanisms of boiler tubes, maintenance practices, and optimum overlays in an effort to reduce boiler tube wastage to a level reasonable for continued efficient operation and reliability.

The optimum overlays will be chosen for the waterwall tubing environment and SH/RH tubing environment based upon the results from testing. The impact angle and velocity, tube surface temperature and erosion resistance, and erodent shape are discussed for each alloy tested. The environment and mechanical properties of the tube surface and erodent are not included. The environment is a very complicated matter. It requires a significant amount of study to describe its effect on erosion, more so on corrosion. Generally, a harder tube surface or higher elastic modulus will provide more erosion resistance. Likewise, more erosion occurs when the erodent has a higher hardness value. Optimum alloys must be selected. The application process also becomes an important factor in how an alloy behaves in service.

The primary sections of this report include:

- Background
- Wear and erosion
- Tested alloys
- Erosion test results
- Repair methods

The background section introduces the user of this document to relevant information pertaining to sootblowers, cleaning media, and damage mechanisms. The four types of sootblowers described include fixed-position blowers, short retractable furnace wall blowers, long retractable blowers, and IK water lance blowers. Each sootblower type includes information on application, typical operating pressures, nozzle diameters, and other areas. Cleaning media commonly employed in sootblowers include superheated or saturated steam, compressed air, water, or combinations of these. The cleaning medium selection is based on application, deposit characteristics, and desired operating pressures among other considerations. Common damage mechanisms are discussed along with the effect of impact variables, condensation effects, identification methods, potential root causes, and prevention measures by maintenance practices.

The wear and erosion section introduces erosion testing methods, mathematical erosion models, and high-temperature material wear data. The erosion testing methods (see *Annual Book of ASTM Standards* [1]) include: ASTM G73-82 "*Standard Practice for Liquid Impingement Erosion Testing,"* ASTM G76-83 "*Standard Practice for Conducting Erosion Tests by Solid Particle Impingement Using Gas Jets*," and additional methods to determine the optimal erosion-resistant alloy. The mathematical erosion models include the cutting model of Finnie and the normal impact model of Mamoun (discussed in detail in Section 3.2). The mathematical models are compared to experimental high-temperature erosion data to compare the accuracy of such models. The section on high-temperature material wear data concentrates on the effects of temperature, thermal and mechanical property versus wear correlations, and alloy erosion and wear data. The alloys evaluated include stainless steels, nickel alloys, carbon steels, tungsten carbide claddings, and thermal-spray coatings.

Twelve alloys were tested for high-temperature erosion resistance. Eleven of the alloys were applied on a SA387 Gr. 11 base metal specimen, and one test specimen was the base metal itself. The alloys used in testing included: nickel alloys (52, 72, 622, 625, 602CA), stainless steels (312, 309L), braze alloy (WC200), and thermal-spray coatings (Cr_3C_2-NiCr, Duocor, and

LMC-M WC blend). A brief description of each coating is provided (if available) including material specification, chemical composition, thermal properties, application process, and cost estimate. The cost estimate serves as an important criterion for selecting the optimal alloy used in a given boiler environment. Sometimes an alloy with a deficiency in performance will be chosen over the more expensive overlay/coating (that is, the ratio of the erosion resistance to cost is higher).

Not all of the application methods noted here are practical for use in the field. Some require coating of tubes or tube panels in a shop application and installation as replacement tubing or panels. Even though one material may provide better erosion resistance than another, its required application technique may make it a less desirable option. The text will indicate which methods can be utilized in the field.

High-temperature erosion testing was performed on the twelve specimens using a particular boiler bed ash as the erodent for testing at the following permutations:

- 900°F (482°C), 30° impact angle
- 900°F (482°C), 90° impact angle
- 1100°F (593°C), 30° impact angle
- 1100°F (593°C), 90° impact angle

The 900°F (482°C) thermal environment represents average metal temperature in waterwall tube sections while the 1100°F (593°C) thermal environment is typical of SH/RH tube metal temperatures. The 30° impact angle is more abrasive of materials that experience ductile-erosion behavior while the 90° impact angle is more abrasive of those that experience brittle-erosion behavior. Therefore, each of the four testing permutations for each specimen must be examined. The data available from high-temperature erosion-resistance testing of the alloys can be sectioned into categories of similar erosion behavior and the optimum alloys can then be determined for the waterwall and SH/RH sections on a performance basis, at 900°F (482°C) and 1100°F (593°C), respectively.

Repair methods are introduced to give the user insight into the application processes commonly employed in tube overlays/coatings. Welding practices, which include gas metal arc welding (GMAW), gas tungsten arc welding (GTAW), plasma arc welding (PAW), and shielded metal arc welding (SMAW) are described. Thermal-spray coating applications, which include the high-velocity oxy-fuel (HVOF), detonation gun (D-Gun), plasma spray, and twin wire arc spray (TWAS) methods are also introduced. Furnace brazing, a shop application technique, is also discussed. Understanding these application techniques is essential in the alloy tube overlay/coating selection process for repair/prevention measures because the application technique is as important as the alloy selection itself.

2
BACKGROUND

The purpose of this section is to establish the appropriate background associated with sootblower-induced erosion. It is unclear if tube wastage in boiler units is caused by direct erosion from sootblowers or an enhanced mechanism known as erosion-corrosion. Primary investigation in this research focuses on the effect of high-temperature erosion. The background information covers the following areas:

- Sootblowers
- Cleaning media
- Damage mechanisms

In macroscopic view, there are the instigators (sootblowers and environment), driving forces (cleaning media), and end results (damage). It is important to discuss each of these areas in sufficient detail to fully understand the physics behind tube wastage. Section 2.1 describes the common sootblowers used in boiler tube cleaning service (emphasizing application, typical operating pressures, nozzle diameters, and other considerations). Section 2.2 discusses the various cleaning media, illustrating application, operating pressures, and in-service comparisons. Common damage mechanisms are discussed in Section 2.3. Additionally, impact variables, condensation effects, identification methods, potential root uses, and prevention measures by maintenance practices are covered in Section 2.3.

Following a detailed discussion of these important topics, the reader is then able to focus more on the technical side of erosion and wear in an effort to select appropriate alloy overlays for tube surface wastage resistance in specific boiler environments.

2.1 Sootblowers

Sootblowers are mechanical devices used for removal of boiler ash and slag deposits on the gas side of boiler tube surfaces. If the gas side of the tube surfaces is not cleaned, excessive fouling occurs, thus creating an extra thermal resistance layer. This layer limits the heat transfer capabilities and, therefore, overall plant efficiency. To limit fouling, it is necessary to periodically clean the surfaces, but not to an extent that creates a corrosion catalyst surface. This environment exists when removal of the protective oxide layer is performed. It can accelerate the erosion damage through an enhanced mechanism known as erosion-corrosion. In addition to removing deposits on tube surfaces, sootblowers also prevent the plugging of gas passages. For further information on optimum frequency of sootblower cleaning, see EPRI technical report *Guidelines for Intelligent Sootblowing Control* [2].

When a high-pressure gas jet from the steam or compressed-air sootblower nozzle expands, it mixes with approximately equal volume of ambient gas for a traveling distance of the nozzle diameter [3]. Therefore, by the time the expanded jet from the sootblower reaches the boiler tubes at a distance between 40 and 100 nozzle diameters, the impacting fluid consists largely of the flue gas. Table 2-1 below gives the number of sootblowers, steam requirement, and operating and impact pressures in a typical 500-MW pulverized coal-fired boiler.

Table 2-1
Sootblowers in Typical 500-MW Boiler [3]

Location	Number of Blowers	Operation (min.)	Steam Consumption Lb_m/min (kg/min)	Steam Pressure at Nozzle psi (MPa)	Impact Pressure psi (kPa)[a]
Furnace	46	0.25	149.9 (68)	145 (1.0)	3.19 (22)
Platen superheater	6	17	291 (132)	101.5 (0.7)	2.32 (16)
Secondary superheater	8	17	187.4 (85)	116 (0.8)	2.61 (18)
Primary superheater	8	11	160.9 (73)	116 (0.8)	2.61 (18)
Secondary reheater	8	17	187.4 (85)	116 (0.8)	2.61 (18)
Primary reheater	8	11	160.9 (73)	116 (0.8)	2.61 (18)
Economizer	4	6	160.9 (73)	116 (0.8)	2.61 (18)
Air heater	8	20	116.8 (53)	101.5 (0.7)	2.32 (16)

[a] For 0.984-in. (25-mm) nozzle at 6.56-ft (2-m) distance.

Sootblower types vary with application and location. However, all sootblowers basically consist of 1) a tube element or lance used to insert into the boiler and carry the cleaning media, 2) nozzles in the tip of the lance to accelerate the cleaning media, 3) mechanical system for mobility, and 4) control system for feedback [4]. Four types of sootblowers are described briefly, including: 1) fixed-position blowers, 2) short retractable furnace wall blowers, 3) long retractable blowers, 4) IK water-lance blowers.

2.1.1 Fixed-Position Blower

The G9B fixed-position blower as shown in Figure 2-1 is a rotating or nonrotating nonretractable sootblower typically used to remove light ash from duct systems or tube surfaces [4]. This type of blower can be used only in areas of low gas temperature and where high mass energy from large nozzles is not required. Fixed-position blowers are much easier to install and operate than

retractable sootblowers. A typical nozzle diameter is 0.3125 inches (7.94 mm), but it can range anywhere between 0.25 inches (6.35 mm) and 0.375 inches (9.53 mm).

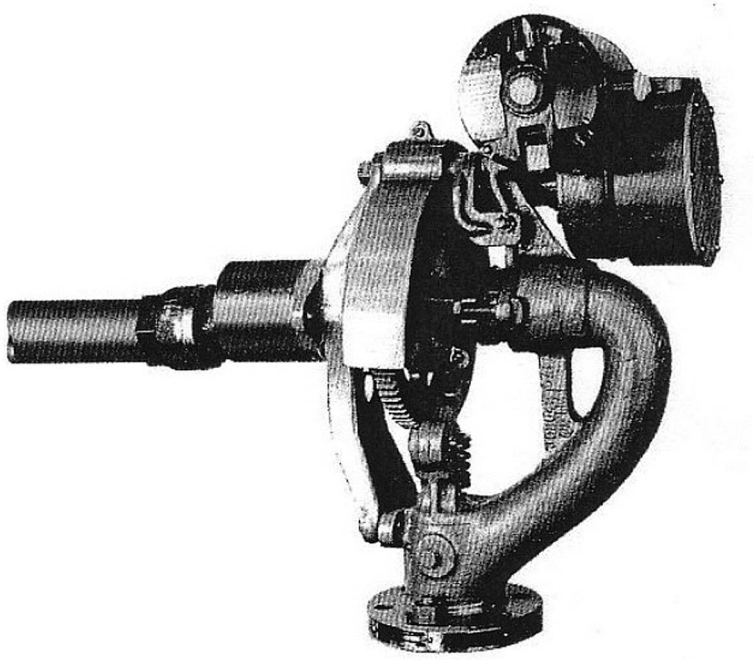

Figure 2-1
Electric Rotor-Driven Rotary Blower [4]

2.1.2 Short Retractable Furnace Wall Blower

A short-travel retractable-type wall blower as shown in Figure 2-2 is used primarily to clean furnace waterwall tubes [4]. The normal nozzle position when the blower is fully extended is approximately 1.5 inches (3.81 cm) from the face of the tubes. The cleaning radius is a function of nozzle pressure, the type of nozzle, the nature of the deposit, and the surface to which the deposit is adhering. Generally speaking, the normal effective cleaning area is an oval with vertical axis of 12 feet (3.66 m) and horizontal axis of 10 feet (3.05 m). The data are based on either gauge air pressures of 150 psi (1.034 MPa) or saturated steam pressures of 200 psi (1.379 MPa). The rotating arc may be diminished from 360° to a lesser degree in order to reduce blowing medium erosion of adjacent sidewall tubes. Nozzle sizes vary, but they are typically on the order of 1 inch (2.54 cm).

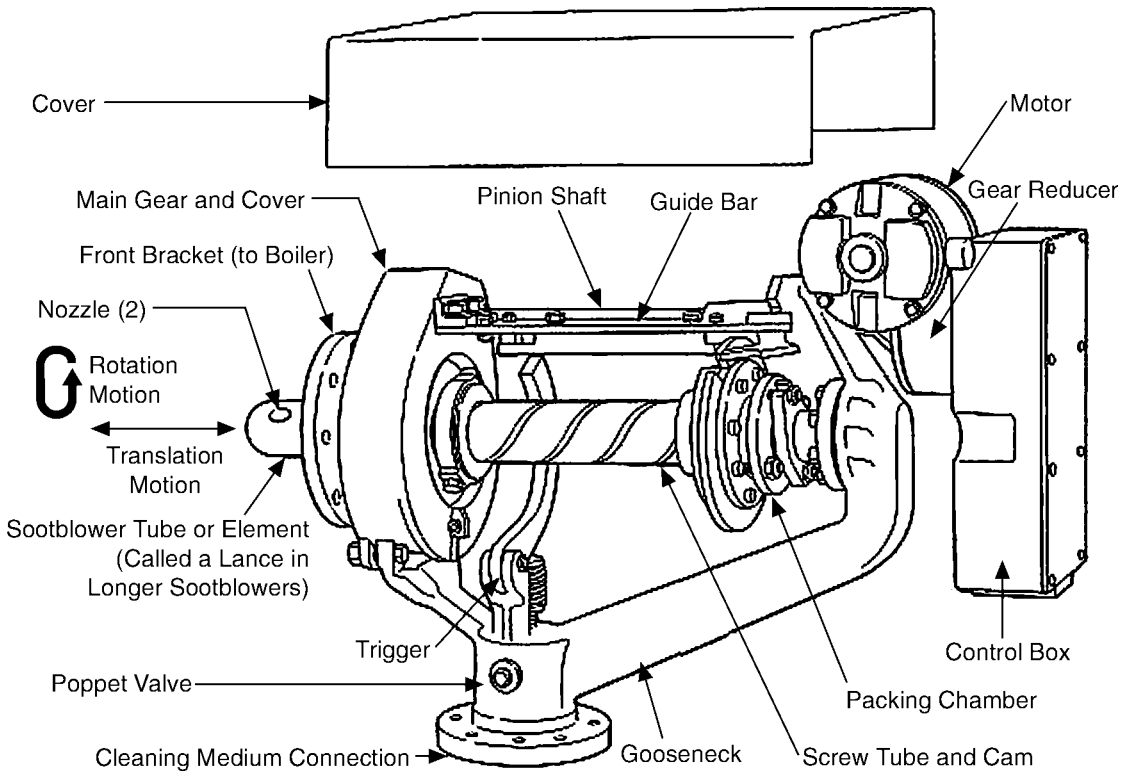

Figure 2-2
Model IR Wall Blower [4]

2.1.3 Long Retractable Blower

An example of a long retractable blower is the model IK-SD as shown in Figure 2-3. This type of cleaning device is used on utility boilers in the SH/RH sections. A long retractable blower contains a set of cleaning media nozzles at the end of the lance that extends into the boiler cavity to clean tube banks and has a travel range of 2 ft (0.61 m) to a maximum of 56 ft (17.07 m). Long retractable blowers are used in vertical or horizontal cavities and incorporate either air or steam as the blowing media. A special nozzle may be used to incorporate water as the cleaning media if deposits are difficult to remove.

The translational speed of the lance varies from 35 in./min (889 mm/min) to as high as 200 in./min (5080 mm/min) [4]. Pressures used in the long retractable blowers are a function of the blowing media, nozzle size, area of application, and fuel deposit characteristics. Typical gauge pressures for air range from 350 psi (2.41 MPa) to 500 psi (3.45 MPa) and steam 70 psi (482.6 kPa) to 350 psi (2.413 MPa). Flow rates are a function of nozzle size, gas zone temperature, and the type of ash being removed. The typical nozzle size for air is 0.625 in. (1.59 cm) and that for steam is 0.875 in. (2.22 cm) or 1 in. (2.54 cm).

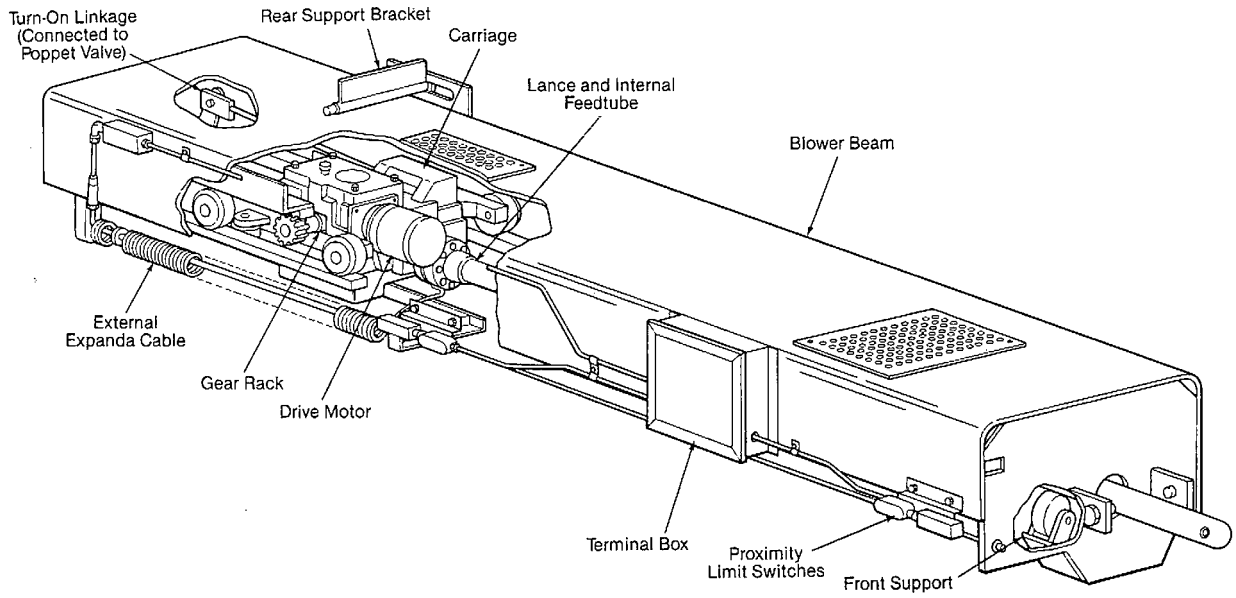

Figure 2-3
Model IK-SD Sootblower - Overall View [4]

2.1.4 IK Water Lance Blower

The IK-4M-WL variable speed water lance blower is typically used when deposits cannot be removed by conventional air or steam as the cleaning medium [4]. The travel speed and rotational speed vary during the cleaning cycle to maintain an optimal water supply for cleaning and to limit the chance of thermal shock in the case of excessive water exposure. Water is typically used in forward motion (insertion) to avoid thermal shock during retracting.

2.2 Cleaning Media

Typical cleaning media used in sootblowers include saturated steam, superheated steam, compressed air, water, or water combinations with other media. Each cleaning medium is selected according to the specific type of sootblower and the nature of the deposits to be removed.

2.2.1 Superheated and Saturated Steam

Superheated steam has become preferable to saturated steam as a field-cleaning medium due to its elimination of moisture [4]. In addition, superheated steam also works better as a cleaning medium on a pound-for-pound basis than saturated steam since it is capable of obtaining a higher sonic velocity through the sootblower nozzle. This increase in sonic velocity more than offsets the effect of having a lower density. Normal gauge nozzle pressures for sootblowers vary from 70 psi (482.6 kPa) to 350 psi (2.413 MPa) for steam, dependent upon the ash deposition removal and sootblower type. Steam may be taken from various sources including superheater headers,

cold reheat inlet headers, secondary superheaters, or hot reheat outlet headers. Each source has its positives and negatives, often influenced by the boiler-operating mode (that is, constant, hybrid, or variable pressure).

2.2.2 Compressed Air

Compressed air is used on larger boilers as a cleaning medium. Typical gauge pressures range from 350 psi (2.41 MPa) to 500 psi (3.45 MPa) on high-pressure reciprocating compressors and 150 psi (1.034 MPa) to 225 psi (1.551 MPa) on high flow rate centrifugal compressors [4]. Multi-stage centrifugal compressors can provide high flow rates at elevated pressures. Normal gauge nozzle pressures for sootblowers vary from 60 psi (413.69 kPa) to 220 psi (1.517 MPa) for air, dependent upon the ash deposition removal and sootblower type.

2.2.3 Water

Water, or any combination of water with air or steam, may also be used as a cleaning medium in sootblower applications. Typically, inlet gauge pressures range from 150 psi (1.034 MPa) to 300 psi (2.068 MPa) [4]. Water injection into sootblowers may be used to cool retractable sootblower tubes or lances that are exposed to high-temperature gas zones. Water blowers are effective in removing slag deposits from fireside waterwall tubes in coal-fired utility boilers [5]. However, repeated thermal shocks from water spraying may damage boiler tubes. The greater the rate of cooling, the higher the thermal stress. Following are several factors that influence the severity of the quench [5]:

- Amount of slag deposit present on tube surface
- Water temperature
- Speed of rotation of the water lance
- Water pressure
- Water volumetric flow rate (gallons per minute)
- Tube temperature prior to the quench
- Cooling rate
- Tensile stresses on tube panel
- Bending stresses on the tube

2.2.4 Cleaning Medium Comparisons

The choice between air, steam, and water as the cleaning medium is dependent upon economic analysis of operating costs and technical issues. The reliability, investment costs, and expected annual operating costs are affected by the following major differences [4]:

- Steam sootblowers must be designed to permit warm-up of system piping, drainage of condensate in the piping, and protection against freezing, corrosion, and erosion. Damage from sootblowers can often be traced back to poor maintenance of the blowing system, including the steam trap system that allows condensate to be blown on the tube surface. The availability of makeup water must also be considered because the condensate from steam blowers is unrecoverable.
- Steam sootblowers typically require more maintenance than air sootblowers, but this cost may be offset by the maintenance cost of air compressors.
- Increasing the capacity of a steam system is typically easy to accomplish because the steam supply from the boiler is normally limited only by pressure-reducing valves. The steam extraction from the boiler represents an available energy loss, but the use of sootblowers outweighs this loss and creates a net energy gain due to an increase in thermal efficiency of the boiler unit.
- Air systems require a higher flow rate than steam systems to cool long retractable blowers due to the lower heat transfer characteristics of air than steam.
- For certain high-temperature ranges in which the deposit strongly adheres to the tube, water may be required as the cleaning medium since neither steam nor air is effective.

2.3 Damage Mechanisms

Waterwall and SH/RH tubes must be cleaned on an as-needed basis in order to maintain or reestablish optimum heat transfer capabilities. When excessive deposits of slag and boiler ash adhere to the boiler tube surfaces, an extra thermal resistance layer is created that lowers the efficiency of the boiler unit. This lower efficiency results because heat must now be passed by means of conduction through a fouling thickness with very low thermal conductivity, thus creating a relatively large temperature drop across the undesired deposit. However, when the tubes are cleaned too often, removal of the protective oxide layer typically occurs, creating a corrosion-catalyst environment favoring surface metal wastage.

Two possible theories exist when examining the damage mechanisms associated with sootblower exposed tube metal wastage. One pertains strictly to erosion and the other is an enhanced mechanism known as erosion-corrosion. The following discussion will introduce erosion, erosion-corrosion, thermal fatigue, embrittlement, condensation effects, impact variables, identification methods, potential root causes, and prevention by maintenance practices.

2.3.1 Erosion

Erosion is caused by the impact, cutting action, or abrasive wear of small solid particles freely immersed in the direction of fluid flow that frequently undercut portions of the material they strike [6]. Erosion conditions are most prevalent in areas where turbulent flow or stream direction changes exist. If high erosion-resistant particles exist in a low erosion-resistant matrix, impacting particles may undercut and remove portions of the material. However, if the high erosion-resistant particles are bound close together in a matrix that does not allow impacting particles to intrude, erosion becomes less of a problem. One function of erosion is the direction in which the particles impact the surface, generally a minimum at 0° and maximum through the 45–90° ranges. Ductile materials experience maximum erosion at 20–30° impact angles, and brittle materials experience maximum erosion at a 90° impact angle.

Waterwall tubes are exposed around one-half their circumference in comparison to full circumference exposure in SH/RH tubes. Therefore, it is obvious that erosion will be experienced in the exposed vicinity. The erosion pattern is a function of the direction of the blow from the sootblower.

In the case that waterwall tubes have little or no ash buildup on the tube surfaces, a distinguishing feature is the formation of fresh rust only a few hours after boiler washing, indicative that the protective scale has been removed [7]. As erosion becomes more profound, tube surfaces begin to thin and flattened areas are created. If internal pressure exceeds that which the thinned region is capable of withstanding, failure occurs.

The rate and extent to which erosion occurs on waterwall and SH/RH tubes is dependent upon several factors. These include particle impact or fluid velocity, angle of impact, particle geometry or composition, erosive resistance, and temperature variations of the tube surface [7]. These are discussed in more detail in the discussion of impact variable in Section 2.3.6.

Erosion does not occur only through solid particle impact experienced through an acceleration of ash particles caused during the sootblowing process. Erosion also occurs when condensed water is immersed in the sootblowing medium. Solid-particle impact or condensed-water impact will have characteristic wear patterns. One way to eliminate condensate in sootblowing media is to incorporate moisture traps. Gouges may occur on tube surfaces due to eddying of the steam between adjacent tubes. Failure generally occurs due to a thinned tube incapable of withstanding the internal pressure. Often the final failure appearance is characterized as ductile and thin-walled. Figure 2-4 provides an example of a high-temperature superheater erosion-damaged tube.

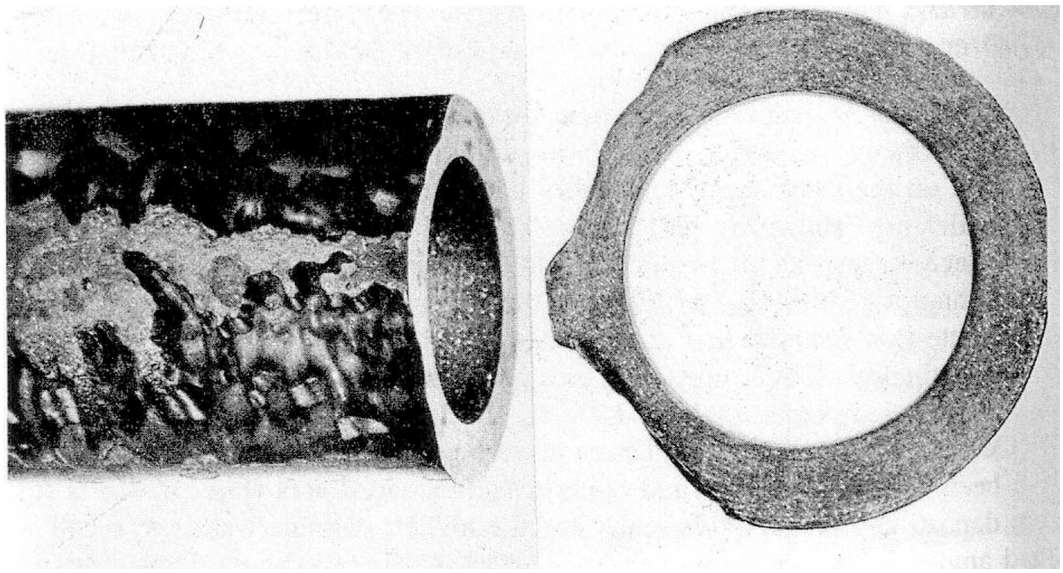

Figure 2-4
High-Temperature Superheater Erosion-Damaged Tube [3]

2.3.2 Erosion-Corrosion

Erosion-corrosion is defined as a corrosion reaction accelerated by the relative motion between a corrosive fluid and the metal surface. This condition typically leads to rather specific cavities in the metal surface, which ultimately creates material wastage such as thinning of boiler tubes. As liquid flows over the surface of a material, it encounters many small irregularities in the normally smooth surface [8]. An example of this is shown in Figure 2-5(a). The fluid begins to cut into the protective film on the surface, removing material as shown in Figure 2-5(b). Eventually these small irregularities grow into large pits as illustrated in the successive illustrations, Figure 2-5(c) and Figure 2-5(d), threatening the integrity of the part.

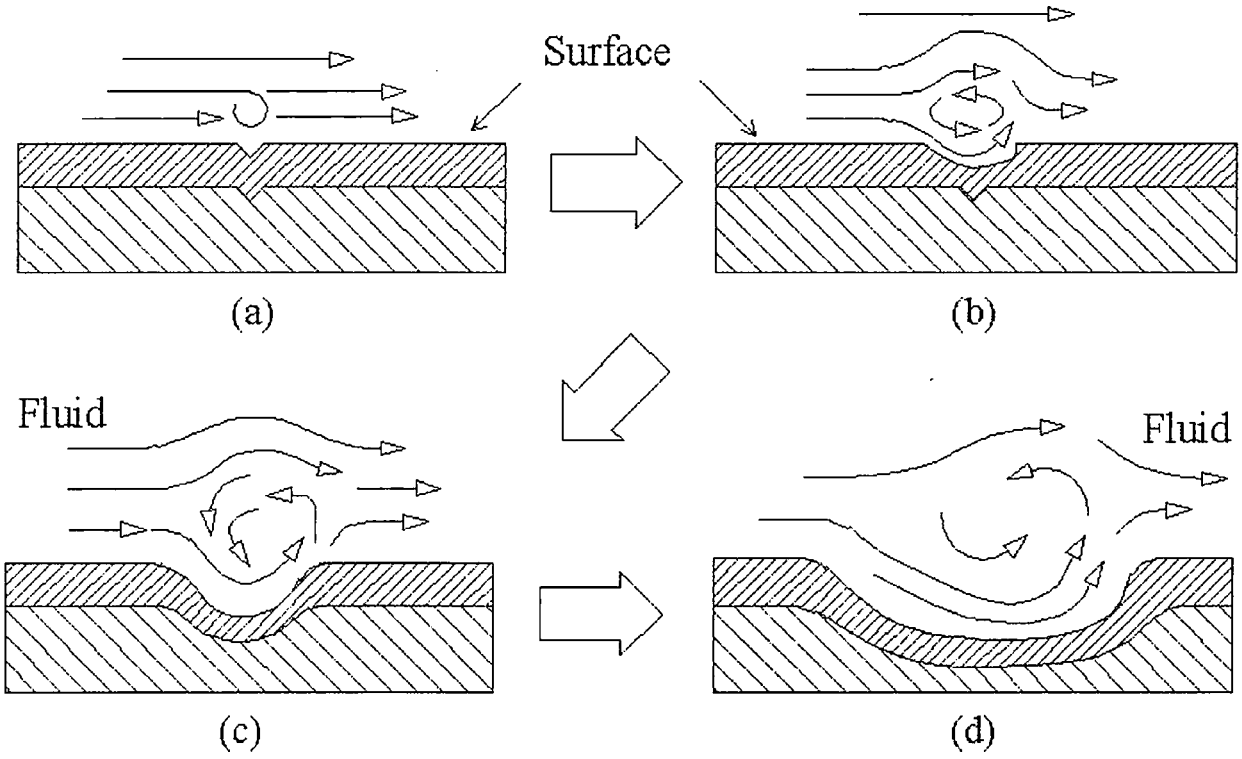

Figure 2-5
Erosion-Corrosion Processes [8]

In the case of turbulent flow, the boundary layer is diminished by swirl motion, which forces the fluid closer to the surface. It is also possible that chemical corrosion increases the damage and rate at which the material is removed. Erosion-corrosion effects appear on the surface of a material as horseshoe-shaped pits, gullies, and grooves, leading to holes that can cause failure such as tube bursting [8]. These grooves and pits exist in a large variety of sizes and tend to grow over the lifetime of the equipment.

Erosion-corrosion is caused by the relative movement between the metal surface and corrosive fluid essentially removing the protective surface oxide layer. After oxide removal, bare metal is exposed to the corrosive fluid, thus causing rapid attack. The combination of entrained particles in the fluid and high flow velocities enhances the possibility for corrosive attack. The attack will vary with increasing velocity up to some limited value at which corrosion accelerates and varies with the smoothness of the metal surface, degree of turbulence, and presence of impurities.

Figure 2-6 is an example of erosion-corrosion failed waterwall tubes in a boiler unit.

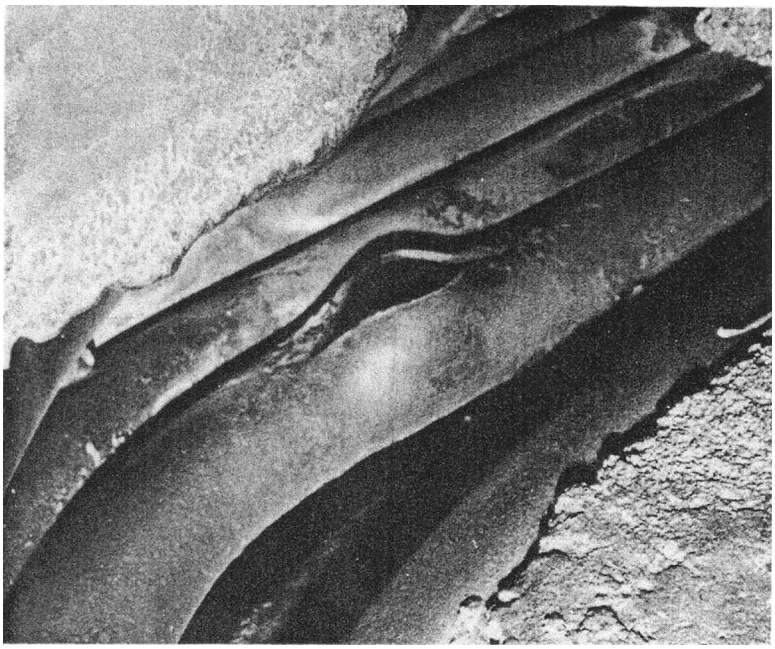

Figure 2-6
Erosion-Corrosion Failed Waterwall Tubes [3]

2.3.3 Thermal Fatigue

Thermal fatigue failure is caused by the cyclic stresses created by thermal expansion and contraction of boiler tubing. Tubes expand with increasing temperature and contract with decreasing temperature. The rate at which this occurs is highly dependent on the material's coefficient of thermal expansion. It is important that the overlay and base metal have similar coefficients of thermal expansion to eliminate failure due to the expansion of one metal more than another. Rapid quenching and heating create high thermal stresses that often create cracking through a cyclic fatigue mechanism when they occur. Thermal fatigue is more profound when sootblowers use water as the cleaning medium. Water has a high specific heat and thus is able to absorb more heat over a quicker time interval than steam or air.

2.3.4 885°F (475°C) Embrittlement

Fine-grained, high-chromium steels generally possess good ductility. However, if held at 750–930ºF (400–500ºC) for long periods of time, they will become harder and embrittled [6]. Embrittled ferritic stainless steels contain two ferrites: one rich in chromium and one rich in iron. Materials with high levels of ferrite are more susceptible to embrittlement. The greater the chromium content in a stainless steel (highest found at Cr contents of greater than 19%), the more susceptible it is to the embrittlement phenomenon. A minimum of 15% Cr is required for embrittlement to occur. The effect of carbon on embrittlement is minimal. High-chromium steels with at least 1% titanium are more susceptible to embrittlement than are similar steels with lower titanium contents. This embrittlement caused by prolonged soaking within the 750–930ºF (400–500ºC) range can be removed only by soaking at somewhat higher temperatures outside this range for several hours. Therefore, although high-chromium contents are highly corrosion

resistant, they can embrittle when exposed to relatively high temperatures for long durations. As the tubes embrittle, they become more susceptible to brittle-erosion failure at impacts normal to the tube surfaces. In addition, embrittlement leads to crack formation, which allows impacting fluid or particulate to undercut and remove sections of the gas-side exposed tube surface.

2.3.5 Condensation Effects

Condensation in air or steam supply lines can result from a variety of sources including improper drainage, temperature variations, insufficient steam superheat temperature, and inadequate aftercooling of sootblower air compressors [7]. If condensate exists in the sootblowing medium, excessively high pressures from the sootblower cause risks for high-impact velocity erosion damage because of the water's high density relative to that of steam or air. Also, thermal shock of the impacted surface is likely to occur due to water's higher capacity to absorb heat than steam or air. This ultimately leads to thermal fatigue cracks in the vicinity of the impacted surface and an easier-to-erode surface. Other issues deal with insulation and heat tracing capabilities. Condensation may be eliminated from the sootblowing system by incorporating moisture/steam traps.

2.3.6 Impact Variables

Erosion caused by sootblowing is dependent upon several variables, which include impact angle, impact velocity, surface material erosion behavior, geometry, and hardness of impacting particles [1]. The impact angle is commonly defined as either the angle between the velocity vector of impact and that normal to the impacted surface (angle of incidence) or the angle between the velocity vector of impact and that tangent to the impacted surface (angle of attack).

Impact velocity is the relative velocity between the surface of a solid body and the impinging fluid or solid particles. In the case of fixed-position tubing, the relative velocity will be only that of the incoming liquid or solid particles. Impact velocity gives a description of the kinetic energy contained in the traveling particles that must be dissipated onto the impacted surface. The greater the velocity magnitude, the higher is the erosion rate.

The nature of material surface erosion will be that of brittle or ductile behavior [1]. Brittle-erosion behavior is characteristic of brittle fracture of the exposed surface. Very little plastic flow occurs, and cracks form that eventually intersect to form erosion fragments. The maximum volume removal usually occurs when the angle of attack is 90° for brittle erosion in contrast to approximately 30° for ductile-erosion behavior. Ductile-erosion behavior is characteristic of ductile fracture of the exposed surface. Considerable plastic deformation occurs by gouging, tearing, or embrittlement as a result of work hardening that leads to crack formation. Two key observable aspects help to identify ductile-erosion behavior. The first is the angle of impact as previously mentioned, and the second pertains to the characteristic ripple pattern that forms on the exposed surface at low values of angle of attack.

2.3.7 Identification Methods

Visual examination can be used to identify many serious erosion problems characterized by excessive tube wastage caused by usage of sootblowers [7]. Visual examination may also identify indirect signs of a problem such as rust locations within a few hours after a boiler wash, indicating the removal of the protective surface oxide layer. Flat areas on the tubing generally identify heavy wastage. Damage should be localized to a circular pattern around the blower. Ultrasonic testing can be used to detect any signs of wall thinning and the degree of associated damage. With this evidence, rational repair or replacement decisions can be made.

2.3.8 Potential Root Causes

Particle-impaction erosion failures are usually reported under three separate headings [3]:

- Fly-ash erosion, mainly in the primary superheaters, reheaters, and economizers
- Sootblower erosion, found in any part of the boiler
- Falling slag impact and erosion, mainly on combustion chamber bottom slopes

Sixty-three fossil-fuel-fired units ranging from 60–1300 MW of output capacity, and the incidents of tube failures from different causes over the period of 1980–1982, are provided in Table 2-2. As shown, fly-ash erosion is the most erosive-natured damage mechanism, followed by sootblower and slag-fall erosion. Depending upon the sootblower cleaning medium (denser is more erosive) and impact velocity (higher is more erosive), sootblower erosion can dominate the erosive damage mechanisms or all tube wastage damage mechanisms listed.

Table 2-2
Tube Failures in Utility Boilers: 1980-1982, Utility A [3]

Cause	Tube Failures	
	Number	Percentage of Total
Fly-ash erosion	195	18.3
Sootblower erosion	82	7.7
Slag fall and erosion	69	6.5
External corrosion	46	4.3
Internal corrosion	27	2.5
Stress cracking	291	27.3
Weld failure	119	11.2
Overheating	158	14.8
Others	79	7.1
Total	1066	-

Background

Erosion induced by sootblowing is caused partly by improper operation and maintenance [7]. This includes improper setting of the blowing temperature, sootblower malfunction, or excessive usage. Table 2-3 lists major root cause influences, confirmation, and corrective actions. Two key actions to identify the particular shortcoming causing boile r tube wear include visual examinations to detect misalignment and calibration/testing to measure parameters such as blower pressures, temperatures, or operation of moisture traps.

Table 2-3
Major Root Cause Influences, Confirmation, and Corrective Action [7]

Major Root Cause Influences	Actions to Confirm	Immediate Actions and Solutions	Long-Term Actions and Prevention of Repeat Failures
• Improper maintenance or operation of sootblowers: — Incorrect setting of blowing temperature (insufficient superheat) — Condensate in blowing media — Improper operation of moisture traps — Excessive sootblowing pressures — Improper location of sootblower — Misalignment of sootblower — Malfunction of sootblower — Excessive sootblowing	• Visual examination to determine obvious maintenance shortcomings or blower problems. • Calibration and testing to measure key parameters: — Blowing temperature and pressure — Operation of moisture traps — Checking travel and sequence times	• Evaluate the extent of wall thinning and erosion damage to determine whether repairs or replacements are required. • Effect applicable repairs or replacements. • Avoid the use of temporary measures such as pad welding unless it is absolutely necessary to get the unit to the next scheduled outage. • Repair sootblower inadequacies and/or modify operation to prevent repeat failures.	• Determine the optimal period of sootblowing. It should not be simply a matter of once/shift or once/day. • Conducting fireside testing with probes to determine the rate of buildup of ash on tubes is useful. • Success has been achieved by having a sootblower maintenance team so that maintenance is performed on a regular basis. • Institute periodic visual examination and a program of calibration and testing of sootblower operation to prevent future failures. • Make needed modifications to hardware or operating procedures to prevent condensate from forming in blowing media.

2.3.9 Prevention by Maintenance Practices

In cases where wall thinning is a significant factor, evaluations should be performed to identify whether the tubes can remain in service or if repair or replacement is required [7]. Generally, repairs are required when the minimum wall thickness specified in the boiler design has been violated. Replacement is necessary if the minimum wall measured is less than 0.100 in. (2.54 mm). Wall thickness below this range cannot typically overlay successfully without burn through or other problems. Using pad welds to increase wear resistance should only be considered as an emergency repair on severely damaged sections to get the unit back in service. They should then be repaired in the next scheduled outage since these measures can induce further problems such as copper embrittlement or flow disruptions if the weld bead happens to penetrate to the inside surface of the tube. If the sootblower problem is not addressed, the result will be repeat failures.

Pad welding is a temporary weld repair on a damaged tube section (that is, a crack in a section of the waterwall tubes) that must be replaced at the next scheduled outage. An overlay is an additional protective layer produced through the welding of an entire bank of thinned tubes to make sure that the minimum wall thickness as indicated previously is always surpassed.

Tube failures by sootblower erosion can be limited through improved maintenance and operation and optimal setting of sootblower parameters and frequency [7]. Some modern boilers have more than 100 sootblowers causing a highly erosive environment. Many utilities have crews set up to perform sootblower maintenance on a regular basis—an optimal approach. It is important to periodically check steam traps and drains to keep water out of the system. In the case of compressed air systems, it is necessary to perform a blowdown of the sootblowing air lines. Thermocouples can be used in steam trap lines to detect any presence of water. If condensate exists in the blowing media, several actions can be taken which include: (1) allow steam to warm-up; (2) completely drain the supply piping through thermal drain valves or impulse condensate drain valves; (3) use an air dryer.

Excessive blower pressure increases the likelihood of erosion since the rate of erosion is dependent upon impact velocity to an exponent of 2 to 4, depending on a number of factors [7]. Bernoulli's equation can be used to relate the sootblower pressure to the nozzle exit velocity—the higher the nozzle pressure, the higher the magnitude of the exit velocity. A reduction in failures will be found in a program that focuses on visual inspection and calibration of sootblowers and their various components, or in a more condensed form so that optimization of operation continues to be achieved. Fireside testing with probes in the area of ash buildup on the tube surfaces may be used to determine the optimum intervals between sootblowing. Sootblowing should not be performed on a once-per-shift or once-per-day interval. It should be performed on a regular basis. Alignment problems may exist due to inadvertent forces encountered during operation. These problems can be found by visual inspection of tubes adjacent to sootblowers during planned and maintenance outages [2].

3
WEAR AND EROSION

The purpose of this section is to introduce sootblower erosion repair on a more technical basis. The following topics are discussed in adequate detail to familiarize the user with the various testing methods and to allow the user to understand important factors behind selecting appropriate weld overlays and thermal-spray coatings for testing:

- Erosion testing
- Mathematical erosion models
- High-temperature material wear

ASTM erosion test methods are introduced including ASTM G 73-82 "Standard Practice for Liquid Impingement Erosion Testing" and ASTM G 76-83 "Standard Practice for Conducting Erosion Tests by Solid Particle Impingement Using Gas Jets*"* [1]. These two common tests allow the user to understand the ways in which a specimen can be exposed to an erosion and/or erosion-corrosion atmosphere. A few examples are used to show erosion results by altering the impact variables, such as target material, impact velocity, impact angle, and the nature of the erodent. Test methods to determine the optimal erosion resistant material are introduced.

Erosion testing is a physical way to test a material's ability to resist erosion. Mathematical erosion models can also be used to illustrate erosion resistance based on theoretical principles. Two of the most widely used mathematical models include the cutting erosion model of Finnie and the normal impact erosion model of Mamoun [9]. A few examples of actual calculated versus experimental erosion rate data are compared in Section 3.2 to show the accuracy of such models.

Section 3-3 (high-temperature material wear) focuses on temperature effects as well as material thermal and mechanical property versus wear correlations. Section 3-3 also contains a case study and incorporates data for various alloys. These alloys include stainless steels, carbon steels, nickel alloys, tungsten carbide claddings, and thermal-spray coatings. Each section will identify specific alloy compositions and wear mechanism data.

3.1 Erosion Testing

The two primary erosion testing procedures mentioned are found in Volume 03.02 of the 1991 *Annual Book of ASTM Standards, Wear and Erosion: Metal Corrosion* [1]. These tests include ASTM G 73-82 "Standard Practice for Liquid Impingement Erosion Testing" and ASTM G 76-83 "Standard Practice for Conducting Erosion Tests by Solid Particle Impingement Using Gas Jets." Section 3.1.1 of this report briefly illustrates these erosion test methods, shows the results from different impact variables, and introduces test methods to determine an optimal erosion

resistant alloy. It should be noted that specific alloys given in this section are used as examples only to illustrate the various ways to conduct erosion testing.

3.1.1 ASTM G 73-82 "Standard Practice for Liquid Impingement Erosion Testing"

This practice concerns testing of solid surface erosion caused by repeated discrete impacts of liquid drops or jets [1]. The objective of the test is to determine the resistance of the material to erosion and to investigate the effect of test variables. A schematic of a small, relatively low-speed, rotating disk-and-jet repetitive-impact apparatus is given in Figure 3-1. One or more test specimens are attached around the periphery of a rotating disk or arm, and various impacts occur between the specimen and liquid droplets.

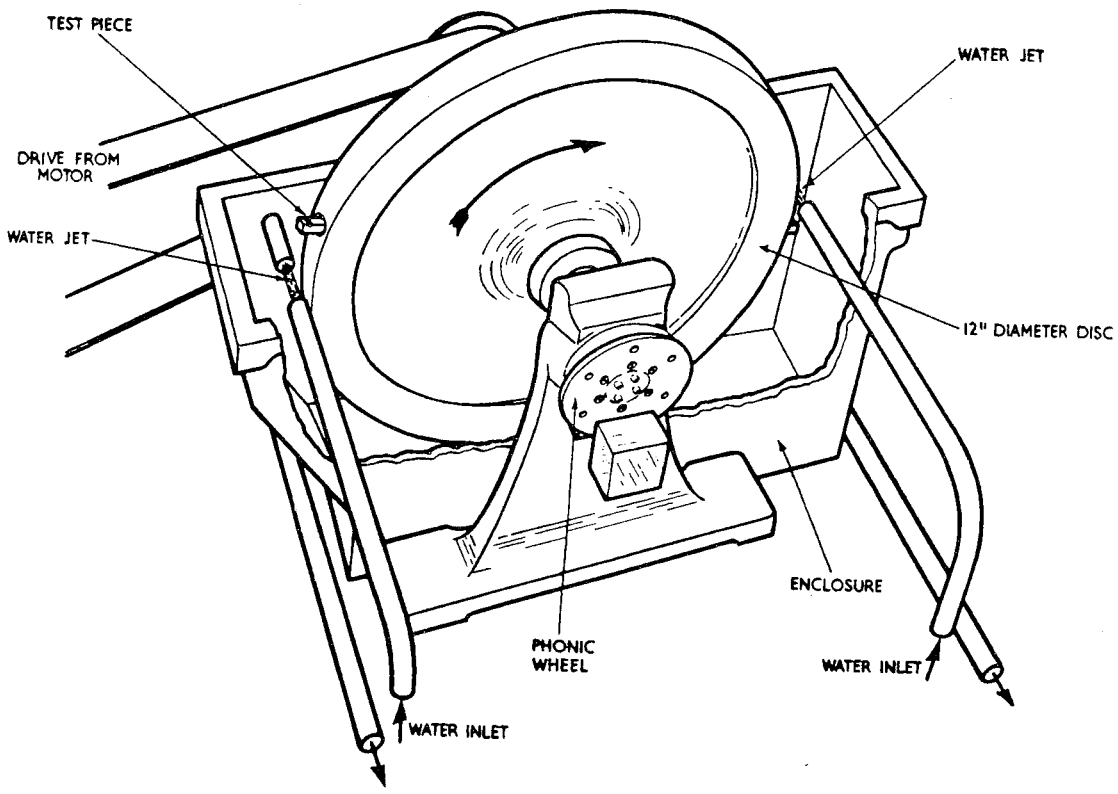

1 in. = 25.4 mm

Figure 3-1
Erosion-Repetitive Test Apparatus Example [1]

An example of a large, high-speed, rotating arm and spray, distributed-impact apparatus is shown in Figure 3-2.

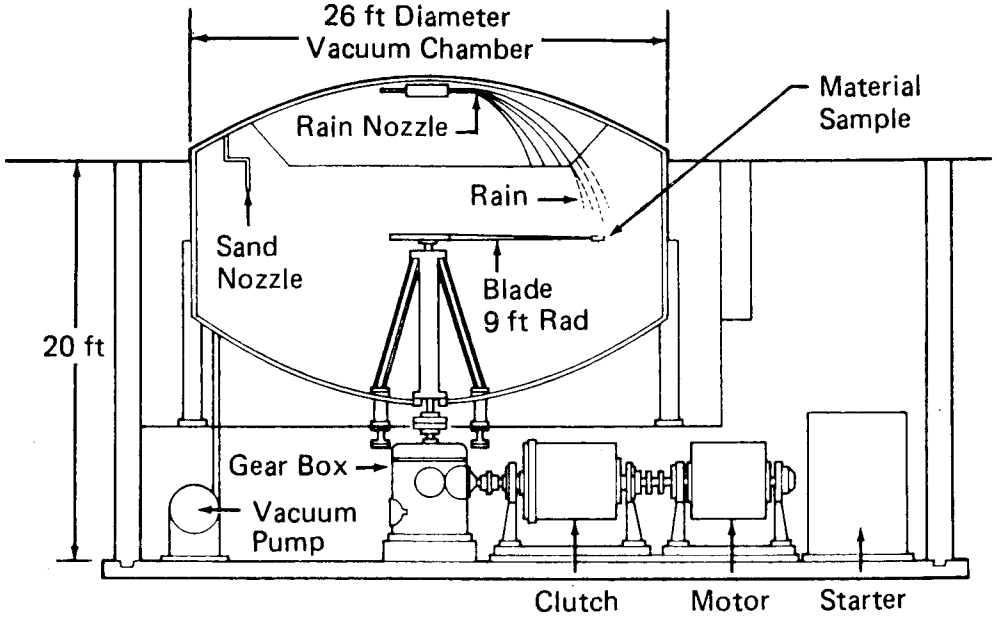

1 ft = 0.3048 m

Figure 3-2
Erosion-Distributed Test Apparatus Example [1]

Devices using sprays or simulated rain fields are characteristic of distributed-impact tests and those using jets are characteristic of repetitive-impact tests. Further information regarding the apparatus, test specimens, test procedures, and calculation of error resistance is available in Volume 03.02 of the 1991 *Annual Book of ASTM Standards, Wear and Erosion: Metal Corrosion* [1].

3.1.2 ASTM G 76-83 "Standard Practice for Conducting Erosion Tests by Solid Particle Impingement Using Gas Jets"

This practice is used to determine the material loss by gas-entrained solid-particle impact erosion with jet-nozzle type erosion equipment [1]. The test is used primarily to determine the solid particle erosion behavior of different materials and acts as a screening test to rank solid particle erosion rates of various materials in simulated service environments. It is limited in that it does not account for a wide range of particle sizes, velocities, attack angles, or environments that exist in actual service. As a result, any laboratory experiment may not be sufficient to evaluate the true performance in service. This practice incorporates repeated impact erosion characterized by a constant stream of gas containing abrasive particles impacting the surface of a test specimen. In the case of sootblowers, a choice of air, steam, water, or combinations of these are used as the stream of gas and the abrasive particles involve the soot buildup on the tube surfaces.

A schematic of solid particle erosion equipment is shown in Figure 3-3. Gas and abrasive particles are mixed in the mixing chamber, delivered through a supply tube, and then accelerated through a nozzle striking the specimen surface through some specified working distance. The material wastage from the specimen surface caused by this impact, primarily measured by weight loss, defines the rate of erosion.

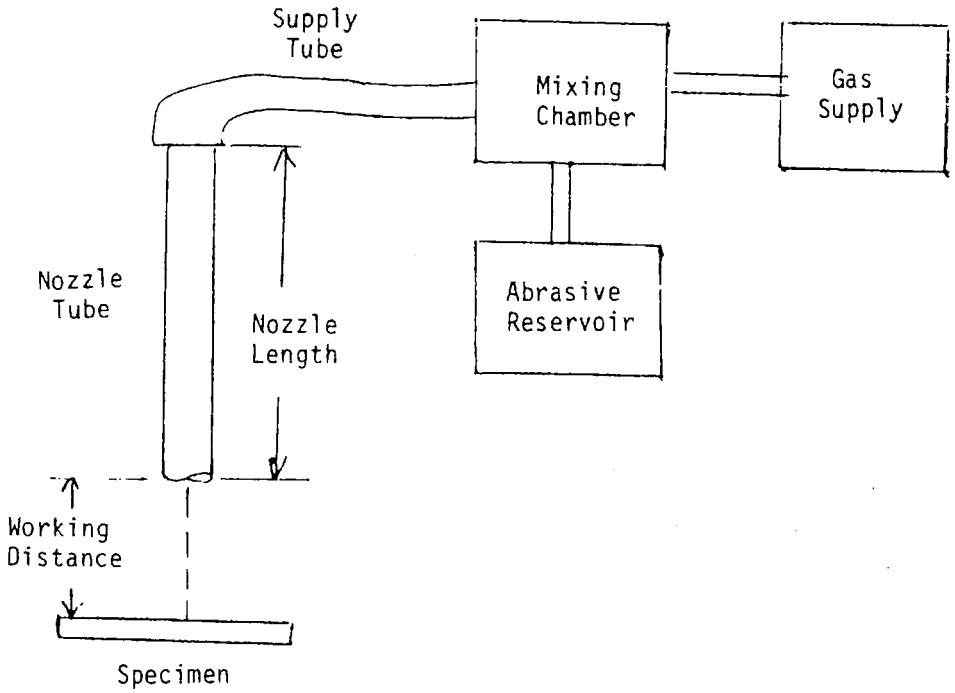

Figure 3-3
Schematic of Solid-Particle Erosion Equipment [1]

More detail regarding apparatus, test materials, conditions, and procedures is available in Volume 03.02 of the 1991 *Annual Book of ASTM Standards*, *Wear and Erosion: Metal Corrosion* [1].

3.1.3 Results from Different Impact Variables

Differing impact variables produce a wide range of erosion rates as will be shown in a few examples. First we will examine an example of erosion versus time for Type 1020 steel at impact velocities of 98.4 ft/s (30 m/s) and 229.7 ft/s (70 m/s). This comparison is shown in Figure 3-4. A few key elements are expanded upon in detail. For example, it is obvious that the greater the impact velocity, the higher is the erosion rate. This becomes more profound as the elapsed time of testing increases.

The impact velocity of a given particle impinging on a surface gives a relation to the total energy that must be dissipated, by means of the kinetic energy defined as one-half the mass times the velocity squared. Realistically, a given particle with mass m, can present a kinetic energy to the surface ratio of approximately 5.44 when comparing the square of the two tested velocities mentioned in the previous paragraph. This kinetic energy must be dissipated. It should be obvious from this analysis that the erosion rate is in some way directly proportional to the energy dissipated onto the surface, hence velocity. The figure indicates impact at a 90° angle where failure typically occurs more in brittle materials. The steady-state erosion rate can be found from the slope of the constant velocity plots, or mass loss divided by time. The average erosion can be

calculated by dividing the erosion rate Lb_m/min (mg/min) by the abrasive flow rate Lb_m/min (g/min) and then by the specimen density Lb_m/in^3 (g/cm^3), resulting in an average erosion value in units of in^3/Lb_m (mm^3/g) [1].

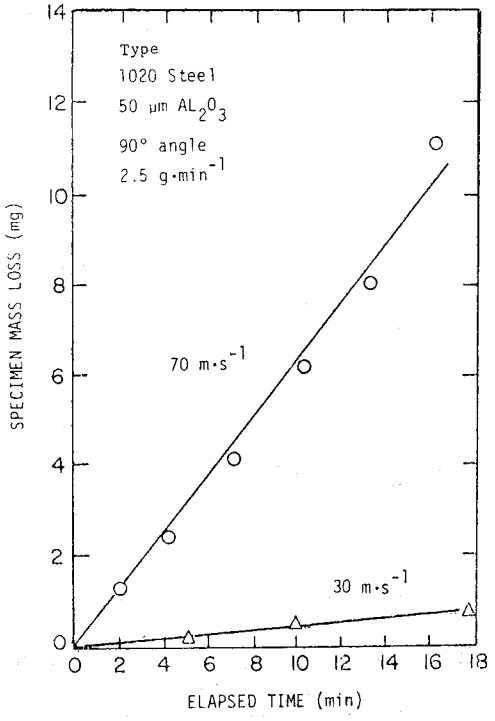

Figure 3-4
Erosion Data for 1020 Steel at 98.4 ft/s (30 m/s) and 229.7 ft/s (70 m/s) [1]

Table 3-1 shows the results of testing three conditions that varied the impacted material type and velocity. Condition A is Type 1020 steel with a velocity of 98.4 ft/s (30 m/s), Condition B is Type 1020 steel with a velocity of 229.7 ft/s (70 m/s), and Condition C is Type 304 stainless steel with a velocity of 229.7 ft/s (70 m/s) [1]. All test conditions have a 0.0044 Lb_m/min (2 g/min) abrasive flow rate, 90° impact angle, and 0.002 in. (50 µm) Al_2O_3 as the abrasive particulate. It should now be clear that Condition B, in comparison to Condition A, would have a greater erosion rate since the impact velocity is greater. Regarding different materials, it can be seen by comparing Conditions B and C, which have equivalent velocities but different materials, that the impacted material also determines the amount of erosion.

Table 3-1
Average Erosion in^3/lb_m (10^{-3} mm^3/g) [1]

Lab Result	Condition A Type 1020 Steel 98.4 ft/s (30 m/s)	Condition B Type 1020 Steel 229.7 ft/s (70 m/s)	Condition C Type 304 SS 229.7 ft/s (70 m/s)
1	6.200×10^{-5} (2.24)	8.719×10^{-4} (31.5)	1.107×10^{-3} (40.0)
2	8.664×10^{-5} (3.13)	6.422×10^{-4} (23.2)	7.031×10^{-4} (25.4)
3	5.896×10^{-5} (2.13)	6.339×10^{-4} (22.9)	7.280×10^{-4} (26.3)
4	1.030×10^{-4} (3.72)	8.968×10^{-4} (32.4)	1.052×10^{-3} (38.0)
5	6.782×10^{-5} (2.45)	8.525×10^{-4} (30.8)	8.885×10^{-4} (32.1)
Avg.	7.584×10^{-5} (2.74)	7.806×10^{-4} (28.2)	8.968×10^{-4} (32.4)

Note: All tests were performed with 0.002 in. (50µm) Al_2O_3 erosive particles, 90° impact, and 0.0044 Lbm/min (2 g/min) abrasive flow rate.

An example of an erosion crater profile for Type 1020 steel eroded at an impact velocity of 229.7 ft/s (70 m/s) and standard conditions otherwise is shown in Figure 3-5. This is the type of pit or groove capable from erosive wear. To have a more accurate depiction of this profile, the width must be stretched five times along its axis to have an equivalent scale to that of the depth axis, thus producing a more realistic image. The maximum depth of this crater profile is approximately 15 mils (380 µm). At this depth and dependent upon sharpness, crack penetration can initiate and through-wall failure is possible if the material thickness is not capable of withstanding the surrounding pressures either through environment or impact. Therefore, it is important to replace or repair this surface to prevent any possible failure mechanisms.

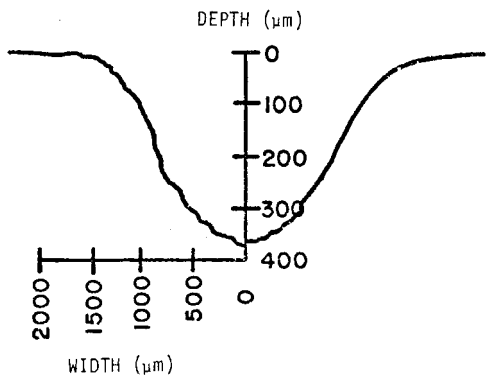

Figure 3-5
Erosion Crater Profile for 1020 Steel Eroded at 229.7 ft/s (70 m/s) [1]

3.1.4 Methods to Determine Optimal Erosion Resistant Alloy

Erosion of fireside boiler tube surfaces is dependent upon several variables, many of which are uncontrollable. The best solution is to test likely weld overlays and coatings for erosion rate versus impact angle. The area under each contour can be used to identify the erosion susceptibility for each of the tested materials.

Another alternative is to test highly researched erosion-resistant specimens at specific angles and temperatures in a common erosion-corrosion environment. The specimens not only depend on the alloy composition, but also on the application process. Applications can be made either by weld overlaying or thermal-spray coatings, some of which have subcategories of application processes within themselves (that is, HVOF thermal spray as discussed in Section 6.2.1 of this report). The most desirable impact angles are 30º for ductile-erosion behavior and 90º for brittle-erosion behavior. Also, temperatures specific to this project's testing will be 900ºF (482ºC) and 1100ºF (593ºC), typical of waterwall and superheat/reheat tubing environments respectively. The results of the tests for each specific temperature should be used to determine the optimum alloys for waterwalls and SH/RH tubing.

3.2 Mathematical Erosion Models

Two mathematical models exist that relate erosion rates to alloy and erodent properties. The methods can be used to test erosion rates in a relativistic manner, but are by no means exact solutions. Erosion rates in service differ with so many variables as is shown by the following mathematical models. (Note: It should be noted that specific alloys given in Section 3.2.3 are used as examples only to illustrate the accuracy of such mathematical models.)

3.2.1 The Cutting Erosion Model (Finnie)

Finnie's model creates an analogy between erosion and cutting wear [9]. For this model, it is assumed that the volume of metal removal is exactly equal to the volume of the crater swept out by the calculated trajectory of the cutting tip through the surface and the width of the cutting face. Every cutting action causes a material loss. The model predicts the cutting erosion as:

$$\text{Vol. Removal} = \frac{cMV^2}{2\psi\rho}\left[\frac{2}{K}\left(\sin 2\alpha - \frac{2}{P}\sin^2\alpha\right)\right] \qquad \text{Eq. 3-1}$$

$$\text{For } \alpha \le \tan^{-1}\frac{P}{2}$$

or

$$\text{Vol. Removal} = \frac{cMV^2}{2\psi\rho}\left[\frac{\cos^2\alpha}{\left(1+\frac{mr^2}{I}\right)}\right] \qquad \textbf{Eq. 3-2}$$

$$\text{For } \alpha \geq \tan^{-1}\frac{P}{2}$$

Where:

C Fraction of particles that cut the surface in the manner assumed by the model

M Total mass of erodent impacting the surface

V Erodent velocity

ψ Ratio of the vertical distance L over which the particle contacts the surface X to the depth of the cut Y_T

ρ Horizontal component of flow pressure between particle and surface

α Angle at which the erodent impacts the surface

$$P = \frac{K}{\left(1+\frac{mr^2}{I}\right)} \qquad \textbf{Eq. 3-3}$$

m Mass of an individual particle

I Mass moment of inertia around its center of gravity

K Constant

r Position

To understand the model visually, a schematic is shown in Figure 3-6:

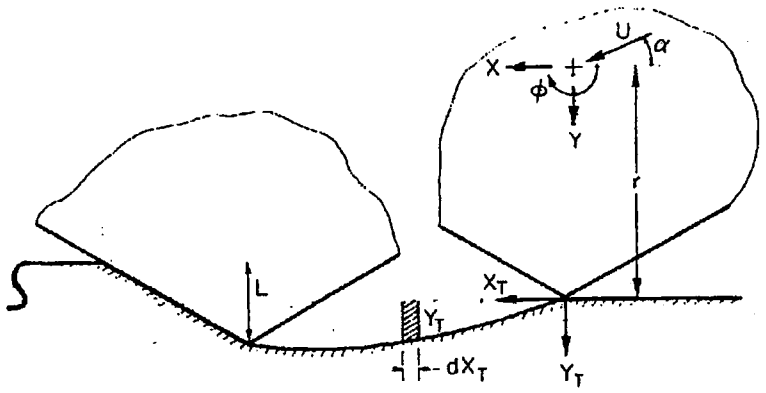

Figure 3-6
Idealized, 2-D Model of a Rigid Particle Cutting Into a Ductile Target [9]

The two equations coincide at tan α = P/2. From grinding data and single grain abrasion tests, Finnie set K = 2, and if I = (1/3) mr^2 (for polyhedral grains), then P = 0.5, so that the expressions coincide when $\alpha = 14°$ [9]. For maximum impacts of ductile targets at 30°, Equation 3-2 is valid and produces an erosion rate given by:

$$\text{Erosion Rate (mg/g)} = d\left(\frac{c}{2\psi\rho}\right)\left[\frac{\cos^2\alpha}{\left(1+\frac{mr^2}{I}\right)}\right]V^2 \qquad \textbf{Eq. 3-4}$$

Where d(g/cm^3) is the density of the impacted material.

Finnie determined that $c/(\psi\rho) = 0.075/Hv$ where Hv is the Vickers Hardness of the eroded area [9]. Assuming c is 0.3 and $\alpha = 30°$, and adjusting for consistent units:

$$\text{Erosion Rate (mg/g)} = 7.172\times10^{-4}\frac{d}{Hv}V^2 \qquad \textbf{Eq. 3-5}$$

Where d is density in g/cm^3, Hv is hardness in kg/mm^2, and V is velocity in m/sec.

Experimental results prove that the exponent of velocity is typically 2.3 or 2.4, or more generally between 2 and 3, rather than 2 as predicted in this model [9]. Equation 3-5 shows that the erosion rate is directly proportional to the density of the impacted material. This makes sense when one takes a look at volume removal—the denser the material, the more mass removed. It is also proportional to the velocity squared, which gives an estimate to the kinetic energy that must be dissipated upon impact—the larger the velocity, the greater the erosion rate. The erosion rate is inversely proportional to the hardness, indicating that the harder the impacted material, the more

resistant it is to erosion. Realistically this model has appropriate variable dependence; however, the exponent on velocity may be a little low, and the resulting equation may be oversimplified in that it depends only on three independent variables.

3.2.2 The Normal Impact Erosion Model (Mamoun)

Mamoun bases his model on derived relationships for erosion rates in response to erosive impacts of the targeted surface [9] For ductile materials, several yield criteria were used to predict initiation of yielding or full plasticity of the impacted surface. Analytical methods were developed to determine the magnitude of the initial impact velocity to cause the volume of the surrounding impact site to experience elastic deflections, the onset of yielding, or full plasticity. The minimum impact velocity to cause fracturing for brittle materials was developed using the Irwin-Griffith criterion for brittle fracture. The concept of a threshold condition was formalized, such as in the case of a strain-hardening ductile material. The expression used to determine the minimum impact velocity (Vip) of a spherical erodent necessary to cause full plastic deformation of the eroded surface is given by the equations below:

$$\mathrm{Vip} = \frac{\left\{\left(\frac{25\pi^2}{3\sqrt{3}}\right)\left[\left(\frac{1-\upsilon_1{}^2}{E_1}\right)+\left(\frac{1-\upsilon_2{}^2}{E_2}\right)\right]^2\left(\frac{Y_{d_2}}{F_y}\right)^3\right\}^{\left(\frac{4+n_o}{2(2+n_o)}\right)}}{\left[0.2^{(2n_o/2+n_o)}(4+n_o)\left(\frac{2\rho_1}{3}\right)(cB_o)^{(2/2+n_o)}\right]^{0.5}} \qquad \textbf{Eq. 3-6}$$

Where

$$F_y = \left\{\left[0.066(1+\upsilon_2)^2 - 0.357(1+\upsilon_2) + 0.48\right]^{1/2} + 0.104f\right\} \qquad \textbf{Eq. 3-7}$$

and

$$B_o = S_{ut_2}\left(\frac{e}{n_o}\right)^{n_o} \qquad \textbf{Eq. 3-8}$$

ν_1, ν_2 Poisson's ratios for the erodent particle and the impacted surface, respectively

E_1, E_2 Modulus of elasticity for the erodent particle and the impacted surface, respectively

Y_{d2} Dynamic yield strength for 8% permanent strain of the impacted surface

η_o Strain-hardening exponent of impacted surface

ρ_1 Mass density of the erodent

c Constant (≈3)

f Friction coefficient

S_{ut2} Ultimate tensile strength of the impacted surface

Mamoun's model assumes that material loss from ductile materials subject to normal impact velocities resulted in elastic deformations only by a fatigue process by way of localized inelastic action or microslip [9]. It was also assumed that the fatigue cracks that resulted after a large number of impacts extended to a depth of about 0.5n, where n is the radius of the circle of the contact made by the erodent on the impacted surface. Assuming that fatigue damage is linearly accumulated, Mamoun was then able to calculate the volume loss/impact:

$$\text{Vol. Loss / Impact} = \frac{\pi}{4} r^3 \left(\frac{1}{N_t} \right) \qquad \textbf{Eq. 3-9}$$

where N_t is defined as either the fatigue life or the probability that an impacted volume becomes detached from the surface. Relating N_t and r to material properties the following expression can be derived:

$$\text{Vol. Loss / Impact} = A \left[\frac{\left(1-\upsilon_1^{\,2}\right)}{E_1} + \frac{\left(1-\upsilon_2^{\,2}\right)}{E_2} \right]^a R_1^{\,b} m_1^{\,c} V_e^{\,d} \qquad \textbf{Eq. 3-10}$$

where

A, a, b, c, d	Calculable constants for a given material
ν_1, ν_2	Poisson's ratios for the erodent particle and target, respectively
E_1, E_2	Elastic modulus for the erodent particle and target, respectively
R_1	Radius of erodent particle
m_1	Mass of the erodent particle
V_e	Initial impact velocity of the erodent particle (less than that required to give plastic yielding)

Incorporating strain-hardening effects into this model yields:

$$\frac{W_L^*}{\Delta n} = \left(\left[\rho_2 \left(\frac{0.4}{I} \right)^{-\frac{1}{\kappa}} \right] \left\{ \left[\frac{(0.5)^{(3+2\eta_o)} 10^{\eta_o} (4+\eta_o)}{cB_o} \right]^{(1-4\kappa)} \left(\frac{\rho_1}{3} \right)^{(1+\kappa\eta_o)} \right\}^{-\frac{1}{\kappa(4+\eta_o)}} V_p^{\left\{ -\frac{2(1-4\kappa)}{\kappa(4+\eta_o)} \right\}} \right) \quad \textbf{Eq. 3-11}$$

where

$W_L^*/\Delta\eta$ Weight loss/erodent impacted, g/g

ρ_1, ρ_2 Mass density of the erodent and eroded surface, respectively

I, κ Dimensionless material constants in $\Delta E_p = I * N_f^{-\kappa}$ where ΔE_p denotes the plastic strain range

η_o Strain hardening exponent of target

c Constant ~3

B_o Flow stress at 100% strain

V_p Initial impact velocity of the erodent particle (greater than that required to produce plastic yielding)

This model is much more rigorous in terms of the number of different variables when compared to Finnie's model. It does not look at only the hardness and density of the impacted surface and velocity of the erodent, but rather takes into account several factors that detail the mechanisms behind material removal (such as the strain hardening exponent of the target, flow stress at 100% strain, and plastic strain range) and important variables of both the erodent and impacted surface. This model is much more detailed in terms of erosion dependent variables and serves as a better model for erosion rate predictions.

3.2.3 Calculated Versus Experimental Erosion Rates

The following data originate from the EPRI report CS-3504, *Erosion-Corrosion of Metals and Alloys at High-Temperatures* [9]. In the report, the Mamoun and Finnie erosion-based mathematical models were used, and the results were compared with experimental high-temperature erosion data in argon and fluidized bed combustion (FBC) atmospheres. As discussed in the report, ten state-of-the-art alloys were tested at different impact angles and velocities to show how erosion wastage varies with the impacted material type, angle, and velocity.

The first comparison between calculated and experimental erosion rates was conducted through analyzing Finnie's model with conditions existing at 1400°F (760°C) [9]. In an argon

atmosphere the series of alloys presented compare to within a factor of 3.3. However, in the FBC atmosphere, the calculated values generally underestimated the erosion rate where oxidation occurred. The improved model where the exponent of velocity is greater than 2 would provide a much better estimate of the erosion rates for most alloys. The comparison for this model is shown in Table 3-2.

Table 3-2
Finnie Model Calculation Versus Experimental Erosion Rates [9]

		Erosion Rate $Lb_m x10^{-3}/Lb_m$ (mg/g)		
Alloy	**Relationship****	**Calculated**	**Experimental**	
			Argon	**FBC**
Stellite 6B	$3.600 \times 10^{-5} V^2$	0.066	0.128	0.227
Stellite 1	$2.548 \times 10^{-5} V^2$	0.046	0.127	0.223
Haynes 25	$3.921 \times 10^{-5} V^2$	0.071	0.116	0.246
Inconel MA 754	$5.291 \times 10^{-5} V^2$	0.096	0.073	0.148
AISI 446	$1.578 \times 10^{-5} V^2$	0.287	0.087	0.106

Note: 30° impact, 1400°F (760°C), 140 ft/s (42.7 m/s), (0. 472 mil) 12µm angular alumina erodent
** V is in m/s corresponding to Equation 3-5

The predicted erosion rates at 1400°F (760°C) 90° impacts based on Mamoun's model were within a factor of 1.3 at best and 29.1 at worst in the argon atmosphere [9]. The primary reason that the model overestimated the rate in every case is due partially to the calculations being made from data at 1600°F (871°C), more commonly found than 1400°F (760°C) data. The fit for the 1400°F (760°C) oxidizing gas erosion was in every case better and between a factor of 1.6 and 4.4, except for AISI 446 where the model overestimated the erosion rate by a factor of 14.5. Table 3-3 shows the calculations based on the Mamoun model versus experimental erosion data.

Table 3-3
Mamoun Model Calculation Versus Experimental Erosion Rates [9]

Alloy	Relationship**	Erosion Rate $Lb_m x10^{-3}/Lb_m$ (mg/g)		
		Calculated	Experimental	
			Argon	FBC
Stellite 6B	$5.79 \times 10^{-10} V^{3.13}$	1.105	0.055	0.334
Haynes 188	$1.45 \times 10^{-8} V^{2.36}$	0.158	0.12	0.25
Inconel 671	$4.48 \times 10^{-9} V^{2.56}$	0.809	0.05	0.24
AISI 446	$2.76 \times 10^{-8} V^{2.464}$	2.444	0.084	0.169
AISI 304	$9.546 \times 10^{-9} V^{2.73}$	0.607	0.099	0.137

Note: 90° impact, 1600°F (871°C), 140 ft/s (42.7 m/s), (0. 472 mil) 12µm angular alumina erodent
** V is in m/s corresponding to Equation 3-11

Mamoun's model fails to take into account embedding and retention of erodent into the alloy surface and by mechanisms of removal other than the fatigue-related mechanism, as suggested by the rippling and other surface features [9]. However, this modeling approach is appropriate for understanding the mechanics of alloy design, and should be extended to simpler cases of erosion at more acute angles than the 90° impacts as shown in the previously discussed testing conditions.

Erosion data are plotted in Figure 3-7 on log-log plots against the material properties such as hardness, modulus of elasticity, yield strength, ultimate strength, melting temperature, Poisson's ratio, strain hardening coefficient, and density. From the plots it is apparent that erosion rate decreases with increasing hardness, elastic modulus, ultimate and yield strengths, melting temperature, strain hardening coefficient, and with decreasing Poisson's ratio (for 90° impacts) for the targeted material. No conclusion can be drawn for the relationship between density and erosion rate. Available literature and Mamoun's model agree with the trends.

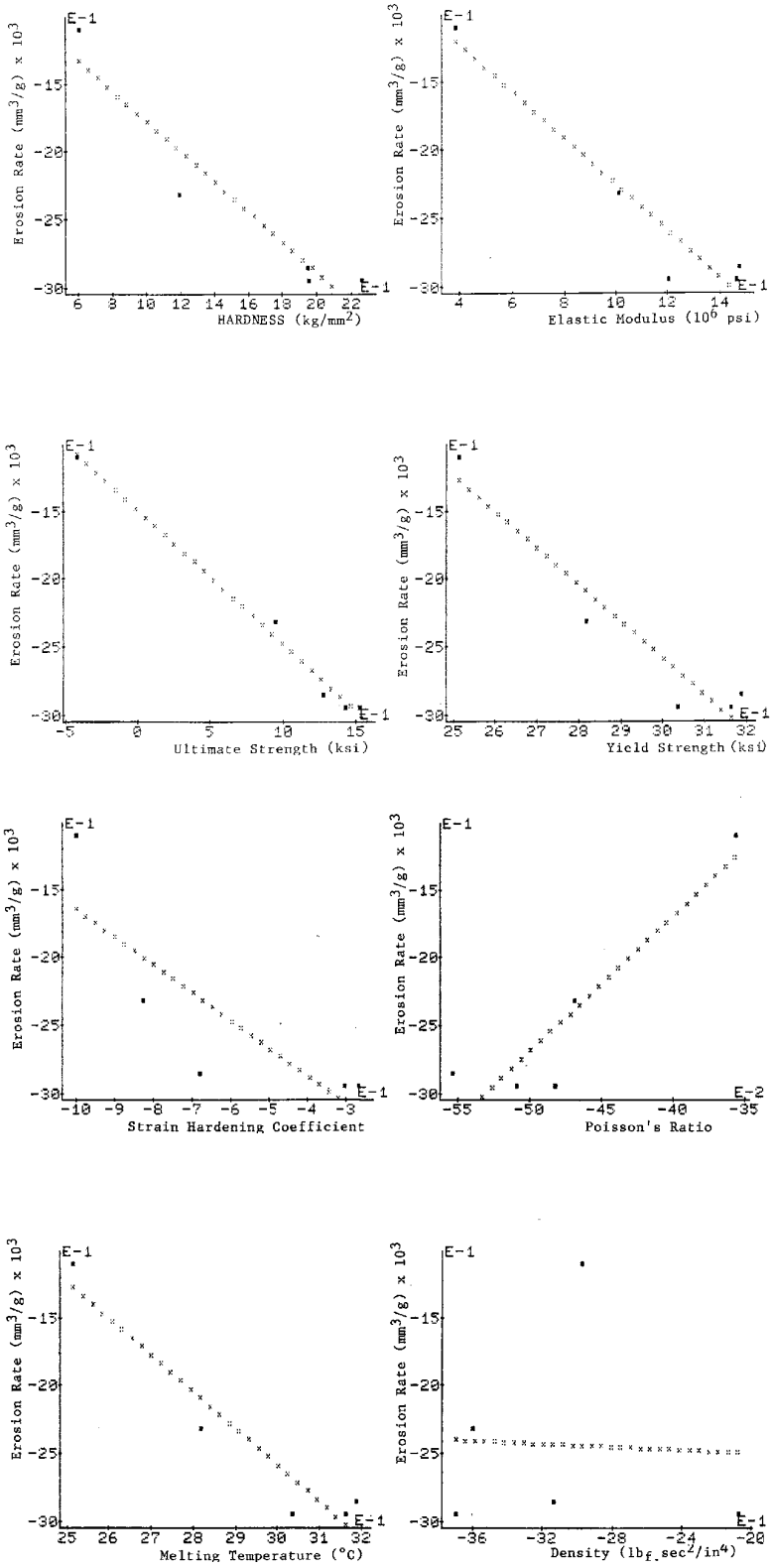

Figure 3-7
Erosion Rates Versus Material Properties [9]

Table 3-4 illustrates the erosion-corrosion behavior in an oxidizing environment for different erodent velocities from 10 different state-of-the-art alloys at 1400°F (760°C). This shows the dependence of erosion on alloy type, velocity, and impact angle.

Table 3-4
Alloy Erosion-Corrosion Rate Data at 1400°F (760°C) [9]

	Erosion Rate $Lb_m x10^{-6}/Lb_m$ (µg/g)				
Alloy	**88 ft/s (26.82 m/s)**	**100 ft/s (30.48 m/s)**	**120 ft/s (36.58 m/s)**	**140 ft/s (42.67 m/s)**	**170 ft/s (51.82 m/s)**
I. Impact Angle Nominally 30º					
Stellite 6B	-43	-30	-80	-218	-410
Stellite 12	-70	-36	-55	-156	-410
Stellite 1	-58	-21	-	-272	-365
Haynes 188	-69	-51	-106	-295	-577
HDA 1675	-62	-46	-121	-279	-597
Inconel 671	-32	-89	-52	-89	-318
Inconel MA 754	-42	-199	-69	-108	-274
Haynes 8077	-58	-110	-66	-281	-272
AISI 446	-51	-83	-47	-141	-231
AISI 304	Oxidizes	-866	+36	-205	-
II. Impact Angle Nominally 90º					
Stellite 6B	-61	-73	-150	-196	-552
Stellite 12	-33	-30	-140	-191	-545
Stellite 1	-59	-81	-150	-206	-
Haynes 188	-52	-65	-187	-258	-552
HDA 1675	-50	-78	-161	-192	-
Inconel 671	-23	-27	-72	-125	-301
Inconel MA 754	-59	-161	-95	-147	-301
Haynes 8077	-59	-158	-92	-165	-242
AISI 446	-44	-224	-151	-157	-
AISI 304	-60	-655	-46	-126	-

Note: All tests performed at 1400°F (760°C) with 0.47 mil (12µm) Al2O3 erodent and simulated flue gas

All alloys presented in Table 3-4 exhibited increasing erosion rate with increasing particle velocity, except AISI 304, whose erratic trends are unclear. The erosion rates can best be described through a statistical fit assuming a relationship [9] of:

$$\text{Erosion Rate (W)} = k[Vp]^n \qquad \textbf{Eq. 3-12}$$

where Vp is the particle velocity and k and n are constants for a given material as shown in Table 3-5.

Table 3-5
Apparent Velocity Exponents of Erosion-Corrosion Rates [9]

		Impact Angle 30º			Impact Angle 90º		
Alloy	**Hardness**	**k**	**n**	**Correlation Coefficient**	**k**	**n**	**Correlation Coefficient**
Stellite 1	257	1.00×10^{-6}	3.9	0.87	2.31×10^{-4}	2.8	1.00
Stellite 12	227	3.13×10^{-5}	3.1	0.85	3.45×10^{-8}	4.6	0.97
HAD 1675	198	1.17×10^{-6}	3.9	0.96	4.01×10^{-4}	3.0	0.98
Haynes 8077	192	1.33×10^{-3}	2.4	0.85	3.99×10^{-2}	1.7	0.80
Stellite 6B	167	5.13×10^{-7}	4.0	0.95	2.04×10^{-5}	3.3	0.98
Haynes 188	167	3.14×10^{-6}	3.7	0.95	2.98×10^{-6}	3.7	0.99
Inconel MA 754	114	4.69×10^{-3}	1.8	0.70	7.77×10^{-5}	1.9	0.80
Inconel 671	110	1.43×10^{-4}	2.8	0.85	2.43×10^{-7}	4.1	0.99
AISI 446	34	3.21×10^{-3}	2.1	0.83	1.02×10^{-2}	2.1	0.57
AISI 304	--	--	--	--	--	--	--

Note: Values of n and k from fitting $\log W / \log V_P$ plots, assuming a relationship $W = k * V_P^n$

It is evident in examining the data that the softer alloys experience a higher erosion rate at 30° impact angles and the harder, more brittle materials experience a higher erosion rate at 90° impact angles. The closer the correlation coefficient is to 1.00, the more accurate the mathematical model is in comparison to experimental results.

3.3 High-Temperature Material Wear

There are two primary theories for the mechanism behind sootblower boiler tube failures—strictly erosion and erosion-corrosion. Stainless steels, carbon steels, nickel alloys, tungsten carbide claddings, and various thermal coatings were investigated to define their resistance to erosion and/or erosion-corrosion. In addition, temperature effects and material thermal and

mechanical property versus wear correlations are discussed. One case study is presented. Material selection plays an important role in limiting the erosion and/or erosion-corrosion damage of boiler tube surfaces. The reason for this is that all other variables are basically fixed and variations will be both relatively expensive and may produce overall lower boiler efficiency.

3.3.1 Temperature Effects

Water blowing of fireside deposits in coal-fired utility boilers creates thermal shock by quenching the tube surfaces. A study was conducted on two panels that were subjected to representative tube surface temperatures, internal pressures, static tensile loads, bending moments, and extremely severe water lancing conditions to produce failures within 50,000–100,000 lancing cycles [10]. The severity was increased by slowing the progression velocity of the lance from a typical 250–300 feet per minute (1.27-1.52 m/s) to 100 feet per minute (0.51 m/s). Another factor in increasing thermal shock is an increase in water pressure and nozzle size, more important at faster progression velocities.

The testing was performed on low-chromium-alloy (SA213-T2) and carbon steel (SA210-A1) tubes [10]. The low-chromium-alloy did not experience significant cracks during the 68,150 lancing cycles. The depth of these cracks did not exceed 0.02 in. (0.51 mm); the wall thickness was 0.27 in. (6.86 mm). The tube surfaces were roughened where direct jet impact occurred and the asperities were well-rounded oxide penetrations or pits, some of which were 0.035 inches (0.89 mm) in diameter. Carbon steel did experience significant cracks during the 68,150 lancing cycles. One of these cracks propagated through the 0.28-in.-(7.112-mm-) thick tube somewhere between 40,000 and 57,000 cycles. The cracks started at deformed grain regions and penetrated transgranularly. After the 68,150 lancing cycles, five of the eight tubes contained cracks in excess of 0.150 inches (3.81 mm). In the carbon steel tubes, circumferentially oriented cracks were deeper than longitudinally oriented ones. For this reason, carbon steel is not considered durable enough for the high-temperature environments that exist in the vicinity of waterwall and superheat/reheat tubes.

3.3.2 Thermal and Mechanical Property Versus Wear Correlations

For steels it is appropriate to relate the hardness of the impacted surface to the erosion wear—the harder the material, the lower the erosion wear. Figure 3-8 shows the relationship between erosion wear of steel alloys of different hardness. As the temperature of the material increases, these hardness values decrease; as a result, the wear rate increases.

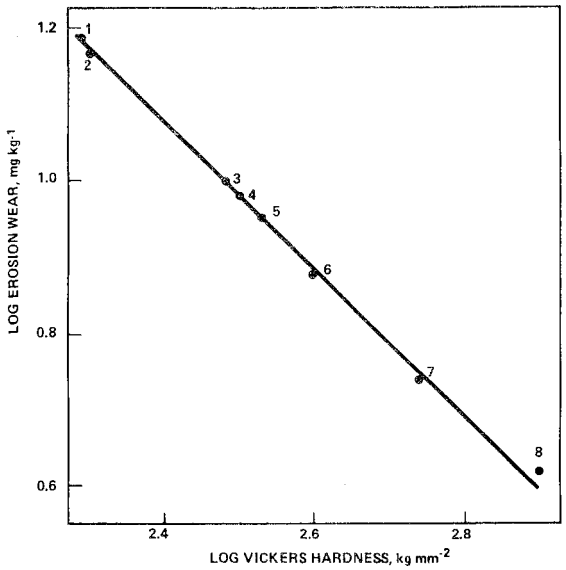

Figure 3-8
Erosion Wear of Steel Alloys of Different Hardness [3]

The materials referenced in Figure 3-8 are: 1) carbon steel; 2) 18Cr 12Ni austenitic steel; 3,4,5,6) carbon steel alloys; 7) Cr-boride hardened carbon steel; and 8) Ni-hard alloy.

The impacting particles are 4.92–5.91 mils (125–150 μm) quartz with a velocity of 90.2 ft/s (27.5 m/s) and angle of impact of $\pi/4$ radians.

3.3.4 Alloys

The section introduces several possible alloys for thermal-spray coatings or weld overlays of waterwall and superheat/reheat tubing. The primary alloys include stainless steels, carbon steels, nickel alloys, tungsten carbide claddings, and thermal-spray coatings. Material composition, available erosion, corrosion, and erosion-corrosion data, and any other relevant descriptions found in the research for optimum alloys in high-temperature boiler environment service are discussed for each. It should be noted that all information on erosion of these materials is from a literature search and not from actual testing. Actual erosion testing of several alloys performed by this project is covered in Section 5 of this report.

3.3.4.1 Stainless Steels

Limited erosion data are available for stainless-steel alloys; therefore, the material performance from a corrosion damage standpoint is introduced for assessment in high-temperature service. It remains unclear as to whether tube wastage in boiler units driven by sootblowers is strictly erosive-natured or erosion-corrosion. Application of stainless-steel overlays in service has shown decreased wear, potentially caused by increased corrosion resistance. Therefore, the corrosion properties of such alloys must be discussed to have a clear understanding of erosion-corrosion damage experienced in waterwall and superheat/reheat tubing.

Stainless steels are iron-based alloys containing a minimum of 12% chromium [11]. Usually the higher the chromium content (can range up to 30%), the greater the corrosion resistance. Corrosion resistance is also a function of the heat treatment, fabrication processing, and surface condition, all of which may change the thermodynamic activity of the surface, thus dramatically affecting the corrosion resistance. It is not necessary to perform chemical treatment on stainless steels to achieve passivity; the passive film forms spontaneously in the presence of air. The following discussion is used to describe the principal alloying elements including chromium, nickel, manganese, and other elements and their effect on corrosion resistance.

Chromium is the one essential element used in forming the passive film or high-temperature corrosion-resistant chromium oxide [11]. Other elements can increase the effectiveness of chromium in forming or maintaining the film, but no other element solely produces the stainless characteristic of stainless steel. The passive film can be observed at about 10.5% chromium with limited corrosion protection, but as the chromium content is increased to 25–30%, the passivity of the protective film is very high, and the high-temperature oxidation resistance is maximized.

Nickel is also critical in that it is used to stabilize the austenitic form of iron and thus produce austenitic stainless steels [11]. It also has corrosion benefits in that it is effective in promoting repassivation, especially in reducing environments. Nickel is particularly useful in promoting increased resistance to mineral acids. When the content of nickel is increased to about 8–10% (a level required to ensure austenitic structures in a stainless which has about 18% chromium), resistance to stress-corrosion cracking (SCC) is decreased. When nickel is increased beyond that level, resistance to SCC increases with increasing nickel content.

Manganese is an alternative austenitic stabilizer. In combination with lower amounts of nickel than otherwise required, manganese will perform many of the same functions as nickel in solution [11]. The effects of manganese on corrosion are not well-documented; however, it is known that manganese combines with sulfur to form sulfides. The morphology and composition of these sulfides have a considerable effect on the corrosion resistance of stainless steels, primarily in their resistance to pitting corrosion.

There are several other alloying elements that influence the corrosion resistance of stainless steels. Molybdenum in moderate amounts, combined with chromium, is extremely effective in stabilizing the passive film in the presence of chlorides [11]. It is also effective in enhancing the resistance to pitting and crevice corrosion. Carbon alone does not seem to play an intrinsic role in the corrosion characteristics of stainless, but it does play an important role by virtue of the tendency of carbide formation to cause matrix or grain-boundary composition changes that may lead to reduced corrosion resistance. Nitrogen is beneficial to austenitic stainless steels by enhancing pitting resistance and retarding formation of the sigma phase. It may help in reducing the segregation of chromium and molybdenum in duplex stainless steels.

The variation of erosion rate with temperature is similar for all types of stainless steels: ferritic, martensitic, precipitation hardening, and austenitic [12]. Erosion rates tend to remain unchanged up to 392ºF (200ºC), rapidly increase up to 1202ºF (650ºC), and then moderately increase up to 1472ºF (800ºC).

The corrosion rate of steels and alloys decreases for steels of more than 25%Cr [13]. Shown in Figure 3-9 are the results of laboratory hot corrosion testing of major austenitic steels reacted with ash mixture of 1.5 mol Na_2SO_4 - 1.5 mol K_2SO_4 - 1 mol Fe_2O_3 at 1202°F (650ºC) for 20 hours in 1% SO_2 - 5% O_2 - 15% CO_2-N_2. It should be noted that steels such as HR3C (TP310HCbN) have the best corrosion resistance among the austenitic stainless-steel family. Alloy 671 (48%Cr - 51.5%Ni) and chromized steel perform best among the tested alloys. Chemical compositions of some of the alloys are presented in Table 3-6.

It is also important in the discussion of stainless-steel alloys to introduce their susceptibility to embrittlement at high-temperatures. For a general discussion of 750–930 °F (400–500 °C) embrittlement, refer to Section 2.3.4.

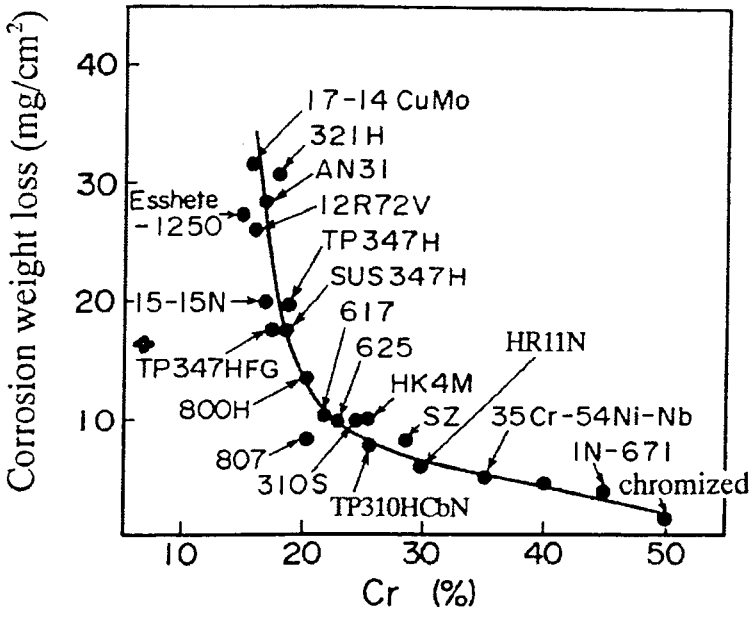

Figure 3-9
Laboratory Hot Corrosion Testing of Austenitic Steels and Alloys [13]

Table 3-6
Typical Compositions of Some of the Alloys Presented in Figure 3-9

Alloy	Ni	Fe	Mn	C	Si	S	Co	Al	Ti	Cr	Mo	P	Nb+Ta	Cu	V	B	N
625	58 min.	5 max.	0.5 max.	0.1 max.	0.5 max.	0.015 max.	1 max.	0.4 max.	0.4 max.	20–23	8–10	0.015 max.	3.15–4.15				
800H	30–35	39.5 min.	1.5 max.	0.05–0.1	1 max.	0.015 max.		0.15–0.6	0.15–0.6	19–23				0.75 max.			
Esshete 1250	9.5	Bal.	6.3		0.5	0.015 max.				15	1	0.035 max.	1		0.3	0.005	
617	44.5 min.	3 max.	1 max.	0.05–0.15	1 max.	0.015 max.	10–15	0.8–1.5	0.6 max.	20–24	8–10			0.5 max.		0.006 max.	
310S	19–22	Bal.	2 max.	0.08 max.	1.5 max.	0.03 max.				24–26		0.04 max.					
IN-671	51.5			0.05						48							
TP347H	9–13	Bal.	2 max.	0.04–0.1	0.75 max.	0.03 max.				17–20		0.04 max.	1 max.				
17-14 CuMo	14	Bal.	0.8	0.1	1				0.2	16.3	2		0.45	3	0.07		
TP310HCbN	20.3	Bal.	1.2	0.06	0.41					24.8	0.01	0.03	0.54				0.23
321H	9–13	Bal.	2 max.	0.08 max.	0.75 max.	0.3 max.			Trace	17–20		0.04 max.					
HR11N	38–42	Bal.	2 max.	0.03 max.	0.6 max.	0.01 max.				27–30	0.5–1.5	0.3 max.					0.1–0.2

3.3.4.2 Nickel Alloys

Because little erosion data were found for these alloys, the following discussion is primarily a corrosion assessment of nickel-based alloys. However, the discussion is important in that it helps in explaining the erosion-corrosion damage of boiler tubing.

Nickel-based alloys are extremely effective corrosion-resistant materials in service environments where temperatures range from subzero to elevated temperatures [11]. They are well-known for their ability to resist severe operating conditions involving liquid or gaseous environments, high stresses, or combinations of these factors. Nickel itself provides excellent corrosion resistance in reducing environments and can be utilized in oxidizing atmospheres that provide the formation of a passive, corrosion-resistant oxide film.

The primary elements used in nickel-based alloys are those containing copper (as in Monels) and chromium plus aluminum (as in superalloys such as Hastelloy or Inconel/Incoloy materials) [11]. Chromium and aluminum provide resistance to elevated temperature oxidation, and chromium and titanium provide resistance to hot corrosion. Chromium is a prime promoter of corrosion resistance in some liquid media at lower temperatures, but other alloy elements such as copper, molybdenum, and tungsten also are quite significant in the enhancement or promotion of corrosion resistance. The following discussion describes the principal alloying elements including chromium, copper, molybdenum, tungsten, iron, silicon, aluminum, and titanium, and their effects on corrosion resistance.

Chromium additions add increased resistance of nickel to oxidizing acids such as nitric and chromic [11]. It also improves the resistance to high-temperature oxidation in binary alloys, provided the chromium level is greater than 5%. When chromium is the element used to provide oxidation resistance, content of 20% or higher is desirable for maximum corrosion protection. Chromium is used in modern superalloys to provide resistance to hot corrosion. Hot corrosion-resistant alloys typically contain 14–22% chromium.

Copper has been a prime alloying element with nickel because the two elements are mutually soluble in one another [11]. Both have good ductility and good corrosion resistance, along with the ability to be hardened. Additions of copper provide improvement in the resistance of nickel to nonoxidizing acids. For example, alloys containing 30–40% copper provide useful resistance to nonaerated sulfuric acid and offer excellent resistance to all concentrations of nonaerated hydrofluoric acid. Also, copper additions of 2–3% to nickel-chromium-molybdenum-iron alloys have been found to produce improved resistance to hydrochloric acid and phosphoric acid.

Molybdenum in nickel substantially improves the resistance to nonoxidizing acids [11]. When molybdenum is used for elevated temperature strength, the hot corrosion resistance of the nickel-base superalloy drastically decreases. Molybdenum in nickel superalloys rarely exceeds 6%; however, a content of 9% has been combined with 21.5% chromium, 3.5% niobium, and minor elements in nickel to produce Inconel 625, a non-age-hardenable superalloy with outstanding resistance to reducing or oxidizing conditions.

Tungsten behaves similarly to molybdenum in that it degrades the hot corrosion resistance of superalloys, but provides improved resistance to nonoxidizing acids and to localized corrosion [11]. Iron is not added to nickel to improve corrosion resistance, but rather to reduce cost. There is potential in the addition of iron in that it does provide nickel with improved resistance to sulfuric acid at concentrations above 50%.

Silicon is typically present in minor amounts as a residual element, restricted to low levels to minimize processing problems and the potential for embrittling reactions in certain alloys [11]. Sometimes silicon is added intentionally to promote the elevated temperature oxidation resistance of superalloys where it probably promotes scale retention of the protective oxides formed by chromium or aluminum.

Aluminum may be added to nickel-based alloys to create high temperature strength through the precipitation of the gamma prime phase in the nickel-chromium matrix [11]. Aluminum also forms oxidation-resistant aluminum oxide scales on alloys that contain greater than approximately 4% aluminum. It may be detrimental in promoting hot corrosion resistance in superalloys, depending on the level of chromium and aluminum in the alloy, in addition to the temperature of exposure to hot corrosion-producing environments. Titanium is found as a constituent of superalloys, where it acts similarly with aluminum to produce strength through gamma-prime hardening.

3.3.4.3 Tungsten Carbide Claddings

Tungsten carbide claddings vary with application requirements. They are designed for maximum wear protection, whether the source is abrasion, erosion, corrosion, impact, or combinations of these wear sources. The dense and hard tungsten carbide claddings are applicable to most surfaces; however, application methods require shop application. It also may not require cladding as thick as other materials due to having a greater density. The application of the tungsten carbide claddings can be accomplished by using proprietary technology involving the formation of a flexible sheet of highly loaded tungsten carbide particles held in a fibrous polytetrafluoroetylene (PTFE) lattice. Infiltration brazing is used to insure a high bond strength and uniform densely packed layer of tungsten carbide, which is encapsulated in a braze matrix chosen for its ability to withstand corrosion and absorb the shock of impact. As a result, bond strengths between the cladding and substrate can exceed 70,000 psi (482.6 MPa). Tungsten carbide claddings have good wear life and wear protection, and are custom-designed for each specific application.

3.3.4.4 Thermal-Spray Coatings

A *Super Hard Steel Elevated Temperature Erosion Test Data Sheet* [14] was developed for tests at 572°F (300ºC), 842°F (450ºC), and 1112°F (600ºC). Waterwall tubes tend to operate more in the 800–950°F (427–510°C) range and superheat/reheat tubing tends to operate more in the 1000–1100°F (538–593°C) category. A summary of the tests conducted at 572°F (300ºC), 842°F (450ºC), and 1112°F (600ºC) follows.

Hot erosion tests of five thermal-sprayed coatings and carbon steel were conducted on a laboratory elevated-temperature erosion tester [14]. The test was conducted at 572°F (300ºC) using a bed ash from an operating CFBC boiler, 197 ft/s (60 m/s) impact velocity, and 30° and 90° angles of impact. The target materials include:

- Arc-sprayed coating (#1)
- JP-5000 HVOF sprayed coating (#2)
- JP-5000 HVOF sprayed fused coating (#3)
- Low-carbon steel
- Arc-sprayed LMC-M
- HVOF sprayed Cr_3C_2-NiCr coating

The thickness losses associated with the five coatings and low-carbon steel specimen are shown in Figure 3-10.

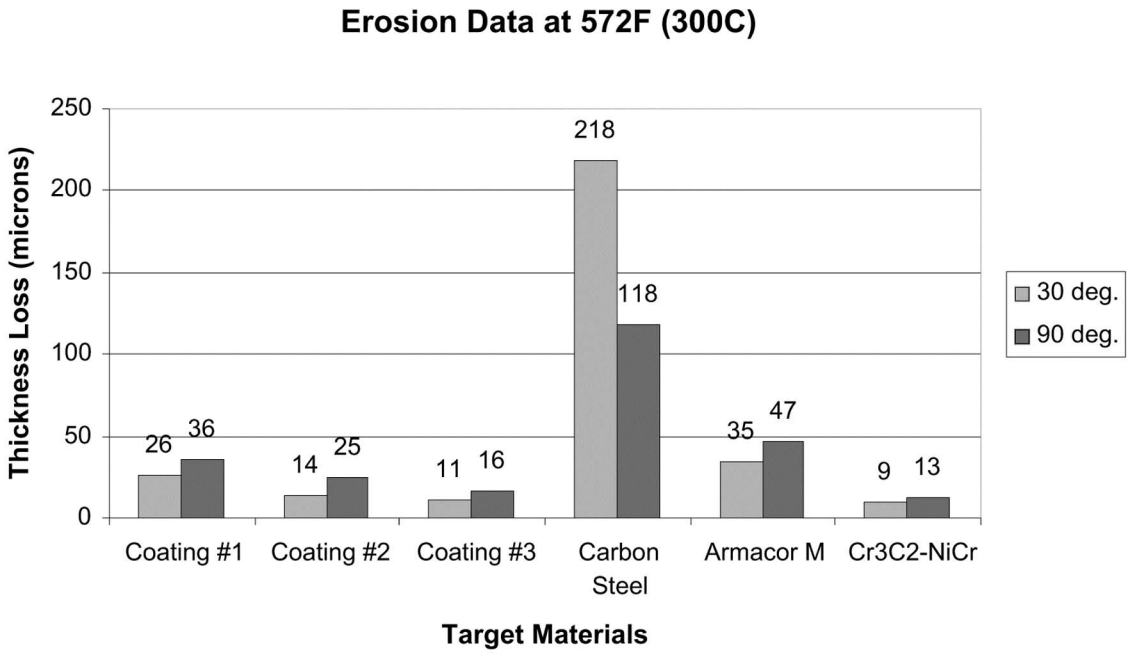

Figure 3-10
Erosion Data at 572°F (300°C) [14]

Hot-erosion tests of three thermal-sprayed coatings were conducted on a laboratory elevated-temperature erosion tester [14]. The test was conducted at 842°F (450ºC) using a bed ash from an operating CFBC boiler, 197 ft/s (60 m/s) impact velocity, and 30° and 90° angles of impact.

The target materials include:

- Arc-sprayed 95 MXC coating (#1)
- Arc-sprayed SHS 717 coating (#2)
- HVOF sprayed SHS 717 coating (#3)

Figure 3-11 shows the thickness losses associated with the these three coatings. Tested at a 90° impact angle, the three coatings had higher erosion behavior than that at 30° impact angle, showing a typical brittle material erosion behavior.

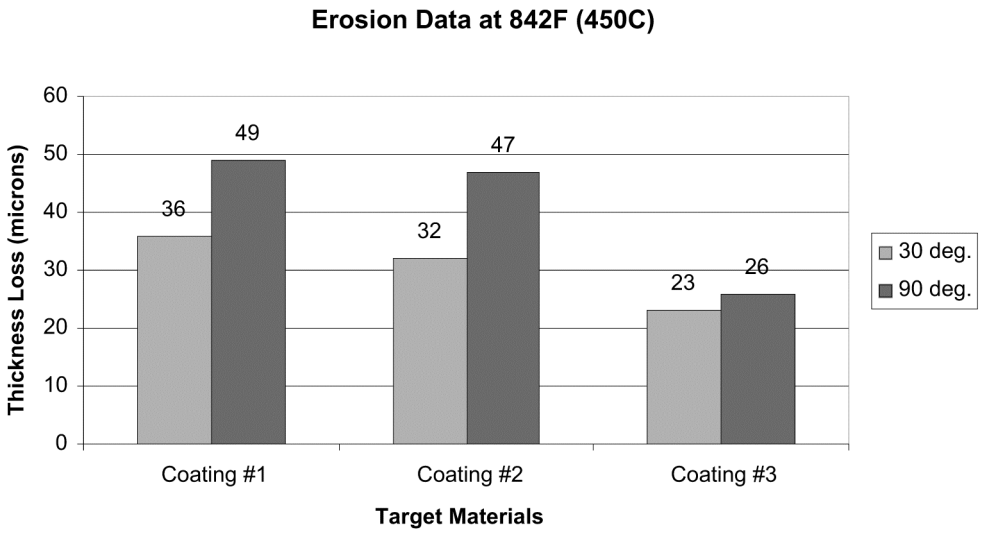

Figure 3-11
Erosion Data at 842°F (450°C) [14]

Hot erosion tests of seven thermal-spray coatings were conducted on a laboratory elevated temperature erosion tester [14]. The test was conducted at 1112°F (600ºC) using a bed ash from an operating CFBC boiler, 197 ft/s (60 m/s) impact velocity, and 30° and 90° angles of impact. The target materials include:

- Arc-sprayed 95 MXC coating (#1)
- JP-5000 HVOF sprayed SHS coating (#2)
- Arc-sprayed SHS coating (#3)
- JP-5000 HVOF sprayed and fused SHS coating (#4)
- Arc-sprayed and fused SHS coating (#5)
- Arc-sprayed Inconel 625 coating
- Cr_3C_2-NiCr coating

Figure 3-12 shows the thickness losses associated with the seven coatings listed.

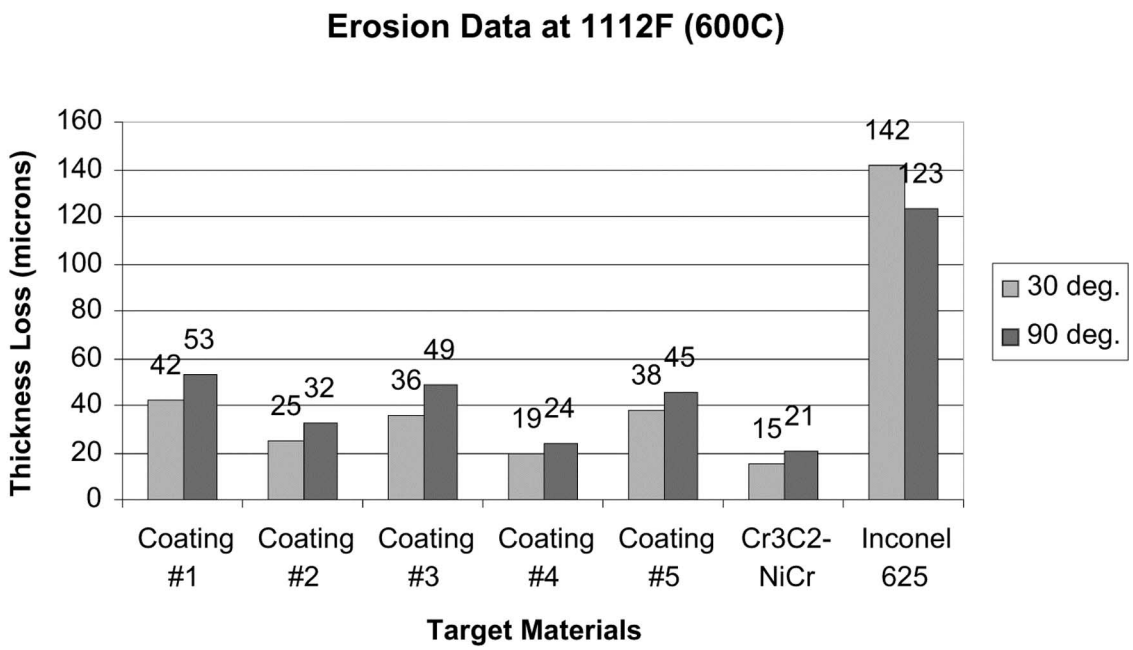

Figure 3-12
Erosion Data at 1112°F (600°C) [14]

The summary of these tests indicates that the Cr_3C_2-NiCr HVOF thermal-spray coating performs better than all those tested in high-temperature erosion service. The identity of the other coatings is concealed and is of no interest in the high-temperature erosion testing conducted in this report. The same type of procedure was performed in testing the selected alloys and those results are presented in Section 5 of this report (Erosion Test Results).

Aluminum metallized coatings (AMC) can be applied on steel tubing to provide protection from high-temperature corrosion up to 1150°F (621ºC) [15]. These coatings can be applied by a variety of means, which include electric-arc, HVOF, and plasma spray. Aluminum is anodic to steel and protects the ferrous substrate in electrolytic solutions. When applied through a non-through porosity thickness, both barrier and cathodic protection are provided. If the coating happens to become damaged and the steel is exposed, the steel will be protected though cathodic protection. Zinc metallized coatings have the same characteristics as that for aluminum, except that aluminum has a higher abrasion resistance. Zinc performs better in alkaline conditions while aluminum performs better in acidic conditions.

Foster Wheeler Development Corporation produced a document in 1998 that describes a waterwall corrosion project coating and overlay performance assessment [16]. The materials tested include thermal-spray coatings, laser-fused overlay, and bare carbon steel, which were used to assess the corrosiveness of the environment. Table 3-11 shows compositions of the materials tested.

Table 3-7
Typical Compositions of Tested Overlay/Coatings [16]

Coating	Cr	Ni	Co	Si	Mn	Mo	Cu	C	B	Fe	Ti	S
LMC-M HVOF	44.5			2.0				0.17 max.	5.9	Bal.	0.7	0.2 max.
XP7 HVOF	27.5	15.3	9.0	1.3		2.4	21.5		3.4	Bal.		
5050 HVOF	43.0	56.0									0.7	
45CT	43.5	55.4		0.02	0.02			0.02		0.4	0.6	0.001
XP7 Laser-fused	27.5	15.3	9	1.3		2.4	21.5		3.4	Bal.		

Twenty-four samples were used, divided into four test groups containing six specimens each [16]. These four groups were made based on permutations of ash covering (ash or no ash) and exposure time (500 and 1000 hours). Table 3-12 distinguishes the group to which each specimen belongs.

Table 3-8
Specimen Coating Permutations [16]

Sample	Base Metal	Coating	Time (hrs.)	Ash Status
Test Group 1				
A1	Carbon steel	LMC-M HVOF	500	No ash
B1	Carbon steel	XP7 HVOF	500	No ash
E1	Carbon steel	HVOF 5050	500	No ash
F1	Carbon steel	45 CT	500	No ash
G1	Carbon steel	Laser-fused XP7	500	No ash
CS1	Carbon steel	None	500	No ash
Test Group 2				
A2	Carbon steel	LMC-M HVOF	500	Ash
B2	Carbon steel	XP7 HVOF	500	Ash
E2	Carbon steel	HVOF 5050	500	Ash
F2	Carbon steel	45 CT	500	Ash
G2	Carbon steel	Laser-fused XP7	500	Ash
CS2	Carbon steel	None	500	Ash
Test Group 3				
A3	Carbon steel	LMC-M HVOF	1000	No ash
B3	Carbon steel	XP7 HVOF	1000	No ash
E3	Carbon steel	HVOF 5050	1000	No ash
F3	Carbon steel	45 CT	1000	No ash
G3	Carbon steel	Laser-fused XP7	1000	No ash
CS3	Carbon steel	None	1000	No ash
Test Group 4				
A4	Carbon steel	LMC-M HVOF	1000	Ash
B4	Carbon steel	XP7 HVOF	1000	Ash
E4	Carbon steel	HVOF 5050	1000	Ash
F4	Carbon steel	45 CT	1000	Ash
G4	Carbon steel	Laser-fused XP7	1000	Ash
CS4	Carbon steel	None	1000	Ash

All samples were placed simultaneously in a furnace at a temperature of 855ºF (457ºC) and exposed to synthetic ash and flue gas [16]. These synthetics were used to simulate the detrimental effects of gas and ash deposit buildups on tube surfaces in actual boiler service. The ash consisted of 20% fly ash, 50% iron sulfide, 10% black carbon, 5% sodium sulfate, 5% potassium sulfate, 5% sodium chloride, and 5% iron chloride. The flue gas consisted of 12% carbon dioxide, 12% carbon monoxide, 6% water vapor, 1000-ppm hydrogen sulfide, and the balance nitrogen. This ash is typical of what would occur on the waterwall of a unit burning high-sulfur coal with low-NO_x burners and suffering aggressive tube wastage.

Based upon qualitative microscopic analysis, the coating rankings for the ash and no-ash environments are as follows: HVOF (LMC-M, XP7, 5050) and arc sprayed (45CT) [16]. The overlay of laser-fused XP7 performed better than the coatings for both environments. Table 3-9 provides a summary of evaluation for the different tested materials after 1000 hours of exposure. The asterisk (*) signifies a thermal-spray coating that was evaluated on the basis of percent-affected coating/base material interface. The percent-affected interface is calculated by taking both wall thickness and penetration into account. The laboratory wastage rate of 88 mils (2.24 mm) per year for the ash environment carbon steel is close to the field-reported result of 80–100 mils (2.03–2.54 mm) per year.

Table 3-9
Summary of Evaluation at 885°F (475°C) for 1000 Hours [16]

Sample	% Affected Interface	
	No Ash	Ash
LMC-M HVOF *	5	10
XP7 HVOF *	10	15
HVOF 5050 *	10	15
45CT *	40	55
Laser-fused XP7 Clad	-	-

* Signifies a thermal-spray coating that was evaluated on the basis of percent-affected coating/base material interface.

Based on Table 3-9, the best material overlay would be the laser-fused XP7 cladding. Following that in the coatings section would be LMC-M applied by the HVOF or twin wire arc spray (TWAS) methods [17]. LMC-M, if applied by TWAS, is characterized by superior erosion and good corrosion resistance, excellent bond strength, and thermal cycling capabilities. It is characterized by a smooth, hard surface offering maximum erosion resistance, non-rusting with excellent performance in salt water, oxidizing acids and caustic solutions, when applied using the HVOF method.

LMC-M is a coating designed to perform well in erosive and corrosive environments to protect boiler operating parts and tube systems [17]. The coating has several benefits such as the ability to extend tube life, being time-efficient to apply and maintain, and working to prevent any unscheduled outages.

Key Performance Benefits of LMC-M

LMC-M achieves hardness levels in excess of 60RC supplying superior erosion resistance, which is maintained at elevated temperatures. LMC-M provides corrosion resistance and spontaneously passivates in the presence of air or oxidizing environments. It is very resistant to sulfidation in boilers. It also provides excellent resistance to thermal cycling by solidifying under compression. The coatings have been cycled over l00 times from room temperature to 1200ºF (649ºC), and the field history has been well-documented regarding its thermal cycling capabilities. There is no heat affected zone (HAZ) as occurs with welding applications; thus, there is no induction of microstructural change, risking cracking that could propagate into the boiler tubes.

The applications for pulverized coal (PC) and fluidized bed boilers [17] include:

- Lower furnace waterwalls
- Nose arches
- Wallblowers/sootblowers
- Screen tubes
- Reheater tubes
- In-bed superheater tubes
- PC superheater tubes
- Sootblower lances

4
ALLOYS TESTED

Defining the erosion and/or erosion-corrosion resistance of alloys is a very complicated task. The evaluation of such alloys can be performed either by developing mathematical models (using theoretical principles) or by performing actual erosion testing. The theory behind erosion and/or erosion-corrosion cannot be fully analyzed by way of a mathematical model because of its great complexity. Therefore, specimens were created for actual high-temperature erosion testing as a way to estimate the erosion-resistance of selected alloys. Twelve alloys were chosen for high-temperature erosion resistance testing. The list was generated through a combination of those typically applied in industry and those found from erosion and/or erosion-corrosion data of carbon steels, stainless-steel alloys, nickel-based alloys, tungsten carbide claddings, and thermal-spray coatings, as presented in Section 3.3.4.

The SA387 Grade 11 alloy steel was chosen for its similarity to the tubing found in common boiler units. It served as the base metal for all alloys tested. The nickel-based and stainless-steel alloys were chosen through a combination of in-service application and erosion and/or erosion-corrosion data. The WC200 braze alloy is Conforma Clad's top erosion resistant coating for the tested boiler environment as shown in Section 3.3.4.3 (tungsten carbide cladding). The Cr_3C_2-NiCr coating was Metalspray's top coating (see Section 3.3.4.4). The Duocor and LMC-M WC blend coatings were chosen by Liquidmetal Coatings to be their most effective wear-resistant coatings in high-thermal environments. The list of alloys for weld-overlay and thermal-spray coatings chosen for high-temperature erosion testing include:

- SA387 Grade 11 alloy steel
- Nickel alloy 52
- Nickel alloy 72
- Nickel alloy 622
- Nickel alloy 625
- Nickel alloy 602CA
- 309L stainless steel
- 312 stainless steel
- WC200 braze alloy
- Cr_3C_2-NiCr coating
- Duocor coating
- LMC-M WC blend coating

Each of these alloys is described based on several aspects including: specifications, chemical composition, thermal properties, application process, and cost. All alloys were deposited on a common SA387 Grade 11 alloy steel base metal. Test results and discussion of the optimum alloys for waterwall and superheat/reheat tubes are presented in Section 5.

4.1 SA387 Grade 11 Alloy Steel

Description

SA387 Grade 11 alloy steel consists primarily of iron and alloying elements chromium, molybdenum, and silicon. Since the chromium level is directly proportional to the alloy's corrosion resistance, this alloy may exhibit significant corrosion damage in high-temperature service. However, since it acts as the base metal for all weld overlays and thermal-spray coatings, it should be tested to show that the overlays/coatings outperform the original base metal.

Specifications

ASME P4 G1
UNS Number K11789

Chemical Composition

Table 4-1
SA387 Grade 11 Chemical Composition Requirements [18]

Element	Weight %	Element	Weight %
C	0.04–0.17	Cr	0.94–1.56
Mn	0.35–0.73	Mo	0.40–0.72
P	0.035	Si	0.44–0.86
S	0.035	Fe	Remainder

Note: All elements without ranges are maximum values

Thermal Properties

Thermal Conductivity [19]: 321.6 BTU-in/hr-ft^2-ºF (46.32 W/mºK) at 68ºF (20ºC)
Coefficient of Thermal Expansion [19]: 6.7 µ-in/in-ºF (12.06 µm/mºC) at 68ºF (20ºC)

Application Process

No application process was utilized. SA387 Grade 11 served as the base metal for the other alloys tested.

Cost

Cost issues that must be taken into consideration include: power, overhead, labor, fabrication/purchase of materials, and lost revenue due to shutdown. The process is primarily a replacement issue, which may be on the higher end of cost in comparison to the coating/overlay applications of the other alloys tested.

4.2 Nickel Alloy 52

Description

Nickel alloy 52 produces corrosion-resistant overlays on most low-alloy and stainless steels [20]. It can be used in applications requiring resistance to oxidizing acids and dissimilar joints involving Inconel and Incoloy alloys and carbon, low-alloy, and stainless steels. It may also be used for weld overlay on steels to establish a protective coating for harsh environments.

Specifications

ASME SFA 5.14, ERNiCrFe-7
UNS Number N06052

Chemical Composition

Table 4-2
Nickel Alloy 52 Chemical Composition Requirements [21]

Element	Weight %	Element	Weight %
C	0.04	Cu	0.30
Mn	1.0	Al[b]	1.10
Fe	7.0–11.0	Ti[b]	1.0
P	0.02	Cr	28.0–31.5
S	0.015	Nb+Ta	0.10
Si	0.50	Mo	0.50
Ni[a]	Remainder	Others	0.50

Note: All elements without ranges are maximum values
a) Includes incidental cobalt
b) Al + Ti is 1.5 max.imum

Thermal Properties

Thermal Conductivity [22]: 93.7 BTU-in/hr-ft^2-ºF (13.5 W/mºK) at 68ºF (20ºC)
Coefficient of Thermal Expansion [22]: 8.44 µ-in/in-ºF (15.19 µm/mºC) at 932 ºF (500ºC)

Application Process

GMAW, also known as metal inert gas (MIG) welding, was utilized for overlaying Nickel alloy 52 on SA387 Grade 11 base metal. The shielding gas was composed of a mixture containing 50% helium and 50% argon gases.

Cost

Costs issues deal with overhead, power, labor, materials, and lost revenue due to shutdown. The cost estimate for Nickel alloy 52 is $22/lb [23].

4.3 Nickel Alloy 72

Description

Nickel alloy 72 is resistant to high-temperature corrosion, including fuel-ash corrosion in atmospheres containing sulfur and vanadium [24]. It also is used for weld overlay protection of base metals such as carbon steels and stainless steels to provide a nickel-chromium alloy corrosion resistant surface [20].

Specifications

ASME SFA 5.14, ERNiCr-4
UNS Number N06072

Chemical Composition

Table 4-3
Nickel Alloy 72 Chemical Composition Requirements [21]

Element	Weight %	Element	Weight %
C	0.01–0.10	Si	0.20
Mn	0.20	Cu	0.50
Fe	0.50	Ti	0.3–1.0
P	0.02	Cr	42.0–46.0
S	0.015	Others	0.50
Ni[a]	Remainder		

Note: All elements without ranges are maximum values
a) Includes incidental cobalt

Thermal Properties

N/A

Application Process

GTAW, also known as tungsten inert gas (TIG) welding, was utilized for overlaying Nickel alloy 72 on SA387 Grade 11 base metal. The shielding gas was composed of 100% argon.

Cost

Costs issues deal with overhead, power, labor, materials, and lost revenue due to shutdown. The cost estimate for Nickel alloy 72 is $22/lb [23].

4.4 Nickel Alloy 622

Description

Nickel alloy 622 is useful for many dissimilar metal joints involving Inconel and Incoloy alloys, and carbon, low-alloy, and stainless steels [20]. The high-chromium content, in addition to molybdenum, produces good resistance to pitting and crevice corrosion. This alloy is also useful for weld overlay on steels for protecting the base metals from harsh environments.

Specifications

ASME SFA 5.14, ERNiCrMo-10
UNS Number N06022

Chemical Composition

Table 4-4
Nickel Alloy 622 Chemical Composition Requirements [21]

Element	Weight %	Element	Weight %
C	0.015	Co	2.5
Mn	0.50	Si	0.08
Fe	2.0–6.0	Cu	0.50
P	0.02	Cr	20.0–22.5
S	0.010	Mo	12.5-14.5
Ni[a]	Remainder	V	0.35
Others	0.50	W	2.5–4.5

Note: All elements without ranges are maximum values
a) Includes incidental cobalt

Thermal Properties

Thermal Conductivity: N/A
Coefficient of Thermal Expansion [22]: .91 µ-in/in-ºF (12.44 µm/mºC) at 68ºF (20ºC)

Application Process

GMAW, also known as MIG welding, was utilized for overlaying Nickel alloy 622 on SA387 Grade 11 base metal. The shielding gas was composed of a mixture containing 50% helium and 50% argon gases.

Cost

Costs issues deal with overhead, power, labor, materials, and lost revenue due to shutdown. The cost estimate for Nickel alloy 622 is $13/lb [23].

4.5 Nickel Alloy 625

Description

Nickel alloy 625 can be used for overlaying to protect the base metal in highly corrosive environments [25]. The nickel and chromium combination provides resistance to oxidizing conditions, and the combination of nickel and molybdenum provides resistance to reducing conditions. The molybdenum content offers resistance to stress-corrosion cracking, pitting, and crevice corrosion.

Specifications

ASME SFA 5.14, ERNiCrMo-3
UNS Number N06625

Chemical Composition

Table 4-5
Nickel Alloy 625 Chemical Composition Requirements [21]

Element	Weight %	Element**	Weight %
C	0.10	Cu	0.50
Mn	0.50	Al	0.40
Fe	5.0	Ti	0.40
P	0.02	Cr	20.0–23.0
S	0.015	Nb+Ta	3.15–4.15
Si	0.50	Mo	8.0–10.0
Ni[a]	58.0 min	Others	0.50

Note: All elements without ranges are maximum values
a) Includes incidental cobalt
** Mil-E-21562E type; Pb<0.010, “Others” include Pb, Sn, and Zn

Thermal Properties

Thermal Conductivity [22]: 68 BTU-in/hr-ft2-ºF (9.8 W/mºK) at 68ºF (20ºC)
Coefficient of Thermal Expansion [22]: 7.11 µ-in/in-ºF (12.8 µm/mºC) at 68ºF (20ºC)

Application Process

GMAW, also known as MIG welding, was utilized for overlaying Nickel alloy 625 on SA387 Grade 11 base metal. The shielding gas was composed of a mixture containing 50% helium and 50% argon gases.

Cost

Costs issues deal with overhead, power, labor, materials, and lost revenue due to shutdown. The cost estimate for Nickel alloy 625 is $11/lb [23].

4.6 Nickel Alloy 602CA

Description

Nickel alloy 602CA exhibits excellent high-temperature creep properties [26]. It is a high-carbon nickel-chromium-iron alloy with additions of micro-alloying elements such as titanium and zirconium together with aluminum and yttrium. 602CA also possesses very good high-temperature corrosion resistance in carburizing and oxidizing/chlorinating media and under metal dusting conditions.

Specifications

UNS Number N06025

Chemical Composition

Table 4-6
Nickel Alloy 602CA Chemical Composition Requirements [26]

Element	Weight %	Element	Weight %
C	0.15–0.25	Si	0.5
Mn	0.1	Al	1.8–2.4
Fe	8.0–11.0	Ti	0.1–0.2
Y	0.05–0.12	Cr	24.0–26.0
Zr	0.01–0.10	Cu	0.1
Ni	Remainder		

Note: All elements without ranges are maximum values

Thermal Properties

Thermal Conductivity [26]: 139 BTU-in/hr-ft2-ºF (20.05 W/mºK) at 1000ºF (538ºC)
Coefficient of Thermal Expansion [26]: 8.2 µ-in/in-ºF (14.76 µm/mºC) at 1000ºF (538ºC)

Application Process

GMAW, also known as MIG welding, was utilized for overlaying Nickel alloy 602CA on SA387 Grade 11 base metal. The shielding gas was composed of a mixture containing 50% helium and 50% argon gases.

Cost

Costs issues deal with overhead, power, labor, materials, and lost revenue due to shutdown. The cost estimate for Nickel alloy 602CA is $16/lb [23].

4.7 309L Stainless Steel

Description

309L stainless steel is similar to 309 stainless steel, except that it has a lower carbon content (0.03% max.) that increases resistance to intergranular corrosion [24]. 309L stainless steel can be used for cladding over carbon or low-alloy steels, as well as for dissimilar joints, to protect the base metal from harsh environments.

Specifications

ASME SFA 5.9, ER309L
UNS Number S30983

Chemical Composition

Table 4-7
309L Stainless Steel Chemical Composition Requirements [21]

Element	Weight %	Element	Weight %
C	0.03	Si	0.30–0.65
Mn	1.0–2.5	Cu	0.75
Fe	Remainder	Ni	12.0–14.0
P	0.03	Cr	23.0–25.0
S	0.03	Mo	0.75
Others	0.50		

Note: All elements without ranges are maximum values

Thermal Properties

N/A

Application Process

GTAW, also known as TIG welding, was utilized for overlaying 309L stainless steel on SA387 Grade 11 base metal. The shielding gas was composed of 100% argon.

Cost

Costs issues deal with overhead, power, labor, materials, and lost revenue due to shutdown. The cost estimate for 309L stainless steel is $5/lb [20].

4.8 312 Stainless Steel

Description

312 stainless steel gives a two-phase weld deposit with a considerably high ferrite content in an austenitic matrix [27]. Even with significant dilution by austenite forming elements (that is, nickel), the microstructure remains two-phase and therefore is highly resistant to weld metal cracks. It can be used to overlay base metals such as low alloy steels to protect them from harsh environments.

Specifications

ASME SFA 5.9, ER312
UNS Number S31380

Chemical Composition

Table 4-8
312 Stainless Steel Chemical Composition Requirements [21]

Element	Weight %	Element	Weight %
C	0.15	Si	0.30–0.65
Mn	1.0–2.5	Cu	0.75
Fe	Remainder	Ni	8.0–10.5
P	0.03	Cr	28.0–32.0
S	0.03	Mo	0.75
Others	0.50		

Note: All elements without ranges are maximum values

Thermal Properties

N/A

Application Process

GMAW, also known as MIG welding, was utilized for overlaying 312 stainless steel on SA387 Grade 11 base metal. The shielding gas was composed of a mixture containing 50% helium and 50% argon gases.

Cost

Costs issues deal with overhead, power, labor, materials, and lost revenue due to shutdown. The cost estimate for 312 stainless steel is $7/lb [20].

4.9 WC200 Braze Alloy

Description

WC200 braze alloy can be applied in a uniform, dense layer of tungsten carbide held in a nickel-chrome-boron braze matrix, which is metallurgically bonded to the component substrate [28]. The tungsten carbide provides erosion and abrasion resistance. The braze matrix, with no interconnected porosity, provides erosion, corrosion, and impact resistance.

Specifications

N/A

Chemical Composition

The approximated chemical composition due to the proprietary nature of the formulation is about 65% tungsten carbide, 30% nickel, and 5% chromium by weight, with small amounts of cobalt, boron, and iron, in descending order of concentration [28]. Custom formulations can be blended for addressing unique wear scenarios.

Thermal Properties

Thermal Conductivity [28]: 234 BTU-in/hr-ft^2-ºF (33.8 W/mºK) at 70-1000ºF (21-538ºC)
Coefficient of Thermal Expansion [28]: 5.4 µ-in/in-ºF (9.72 µm/mºC) at 1000ºF (538ºC)

Application Process

The application process involves adhering two cloth-like films, one containing the tungsten carbide particles in an organic binder and the other the brazing alloy (WC200), to the part to be cladded (SA387 Grade 11), and then furnace-brazing to impregnate the pores in the tungsten carbide with brazing compound to form a metallurgical bond between the braze lattice and the substrate [28]. This unique flexible-cloth process allows for protection of very complex component geometries, including tight radii. It also facilitates the application of custom cladding thicknesses in order to target specific areas of wear. For components that cannot be directly cladded in the vacuum furnace, the manufacturer can fabricate custom wear liners to be applied to components.

Cost

Cost varies widely depending upon multiple factors including size of the component to be protected, complexity of the component geometry, surface area-to-volume ratio of the component, post cladding (braze) heat treatment requirements, thickness of the desired cladding application, and specifics of formulation customized to specific application requirements. The cost range can vary between $1.50–$5 per square inch. However, for a unique cost estimate of the cladding itself, the user should contact Conforma Clad, Inc.

4.10 Cr_3C_2-NiCr Coating

Description

Cr_3C_2-NiCr is a chromium-carbide metal cermet coating, which exhibits higher levels of erosion resistance when the composite powder possesses finer structure, more uniform distribution of NiCr particles, lower porosity and oxide rate, as well as higher micro hardness values than that of the blend powder [29]. The coating exhibits nominal values such as porosity less than 1%, oxide rate less than 4%, with bond strength about 5.80 ksi (40 MPa), and hardness HV_{300} 714.

Specifications

N/A

Chemical Composition

The nominal composition is about 70% chromium carbide and 30% Nichrome (NiCr) [29].

Thermal Properties

Thermal Conductivity [29]: 123.4 BTU-in/hr-ft^2-ºF (17.8 W/mºK) at 932–1112 ºF (500–600 ºC)

Coefficient of Thermal Expansion [29]: 6.17-6.28 µ-in/in-ºF (11.1-11.3 µm/mºC) at 932–1112 ºF (500–600 ºC)

Application Process

The Cr_3C_2-NiCr coating was sprayed via HVOF using a special composite powder with carbide activating technology onto a SA387 Grade 11 base metal [29].

Cost

For a detailed cost estimate of the coating and application, the user should contact Metalspray, Inc.

4.11 Duocor Coating

Description

Duocor coatings are applied by thermal-spray wires, which utilize titanium and tungsten carbides within an amorphous matrix for high-stress abrasion resistance [17]. Applications include pumps, non-skid flooring, and boiler high wear zones.

Specifications

N/A

Chemical Composition

Table 4-9
Duocor Coating Chemical Composition Requirements [30]

Element	Weight %	Element	Weight %
Fe	Remainder	Mn	4
Cr	20	Ni	6
Si	3	Tungsten Carbide	25
B	6	Titanium Carbide	6

Thermal Properties

N/A

Application Process

A Duocor coating (0.035-in.-[0.89-mm-] thick) was applied by way of TWAS onto a SA387 Grade 11 base metal.

Cost

For information on application and a detailed cost estimate of the coating materials, the user should contact Liquidmetal Coatings.

4.12 LMC-M WC Blend Coating

Description

The LMC-M WC blended coatings are smooth, hard surfaces offering maximum erosion resistance, non-rusting with excellent performance in salt water, oxidizing acids, and caustic solutions [17]. Applications include agricultural blades, roll dryers, pressure rolls, capstan, and boiler tubes. The LMC-N with WC blend material evaluated in this paper is a prototype material only and is currently under development for applications requiring a tough abrasion resistant coating.

Specifications

N/A

Chemical Composition

The chemical composition of the LMC-M blend coating is not well known. However, it is a blend of LMC-M self-fluxing powder (chemical composition is shown in Table 4-10) and tungsten carbide, which was blended at an unknown ratio.

Table 4-10
LMC-M Powder Chemical Composition Requirements [30]

Element	Weight %
Fe	Remainder
Cr	50
Si	3
B	8
WcW2C	Cast/crushed tungsten carbide, 25%

Thermal Properties

N/A

Application Process

A LMC-M WC blend coating (0.035-in.-[0.89-mm] thick) was applied through a low-cost highly portable JP5000 HVOF device onto a SA387 Grade 11 base metal [31].

Cost

One pound of the LMC-M WC blend alloy, for large jobs, would cost $18-$20 [31]. However, the price variation is directly linked to the quantity purchased. Other requirements such as those presented in Section 4.11 should also be addressed for an accurate cost estimate. For information on application and a detailed cost estimate of the coating, the user should contact Liquidmetal Coatings.

5
EROSION TEST RESULTS

High-temperature erosion testing was performed on the twelve alloys presented in Section 4. This section is used to describe the test setup, results, and optimum alloys for both waterwall and superheat/reheat tubing solely on a performance basis.

5.1 Test Setup

The high-temperature erosion tests were carried out using the bed ash from an operating boiler as the erodent material. As shown in Figure 5-1, the particles were a mixture of both round and angular shape with a mean particle size of 21.9 mils (556 microns) and mean particle density of 164.4 Lb_m/ft^3 (2634 kg/m^3). The particle distribution of the bed ash is given in Figure 5-2. The particles were comprised of high concentrations of silicon and calcium with minor concentrations of aluminum, magnesium, sulfur, iron, phosphorous, titanium, and chlorine. An EDS analysis of the bed ash particles is shown in Figure 5-3, with the amplitude of the peaks being proportional to the particulate concentration.

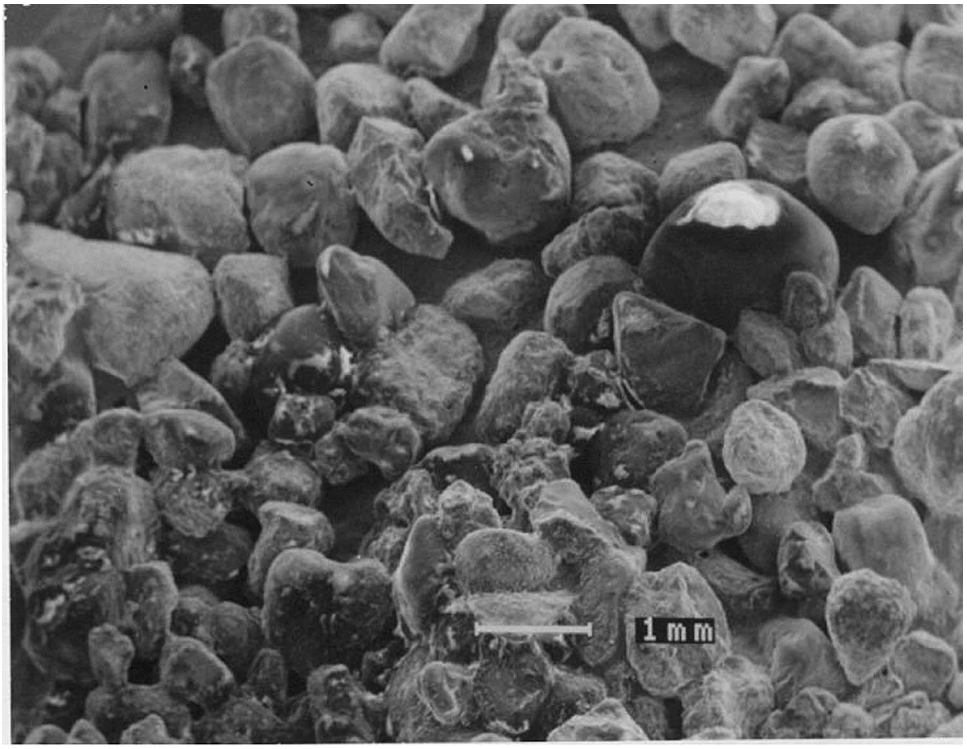

Figure 5-1
Bed Ash Appearance [32]

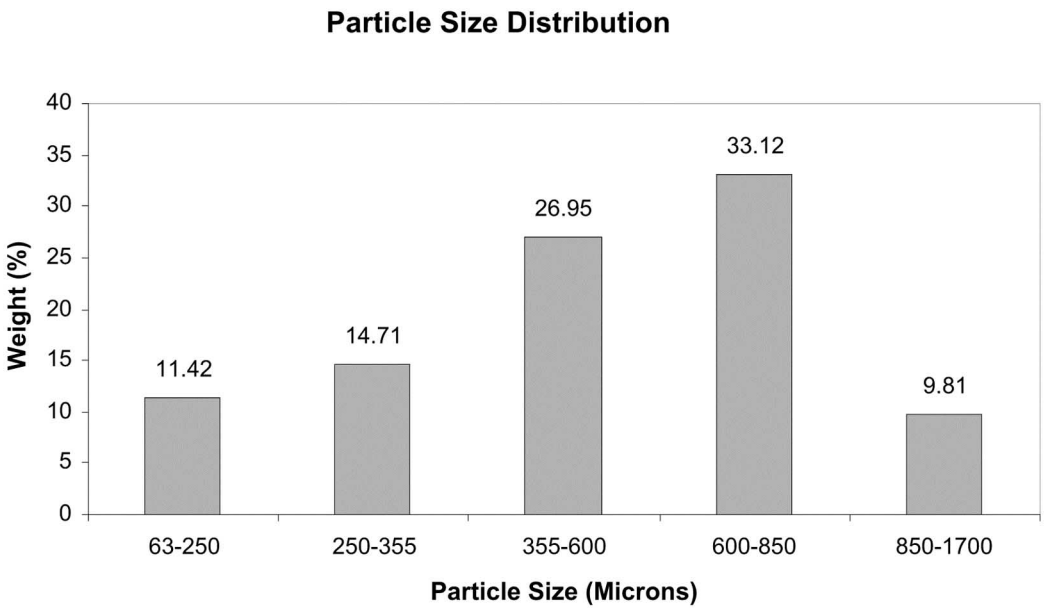

Figure 5-2
Bed Ash Particle Distribution [32]

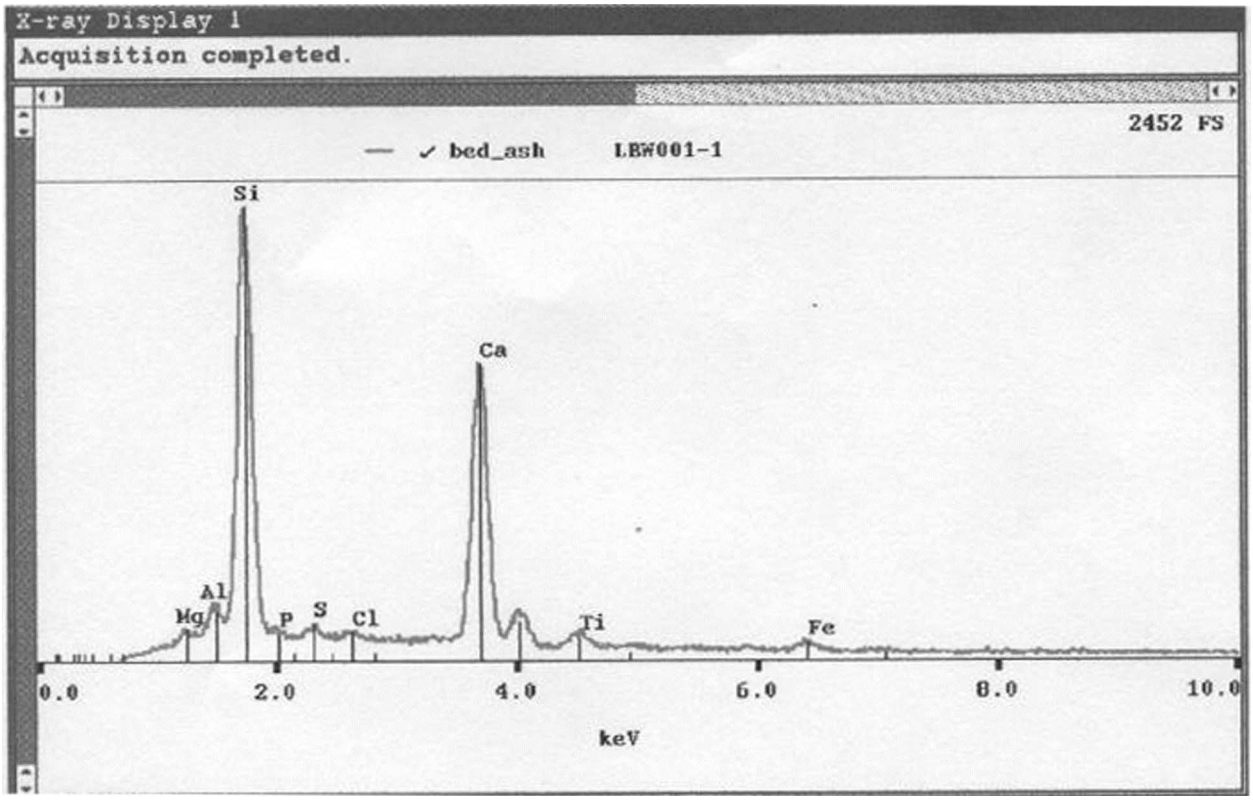

Figure 5-3
EDS Analysis of Bed Ash Particles [32]

The base metal was SA387 Grade 11 alloy steel and the target materials and corresponding application process used for testing purposes are given below:

1. SA387 Grade 11 alloy steel - no application
2. Nickel alloy 52 - GMAW
3. Nickel alloy 72 - GTAW
4. Nickel alloy 622 - GMAW
5. Nickel alloy 625 - GMAW
6. Nickel alloy 602CA - GMAW
7. 309L stainless steel - GTAW
8. 312 stainless steel - GMAW
9. WC200 braze alloy - infiltration brazing
10. Cr_3C_2-NiCr coating - HVOF
11. Duocor coating - TWAS
12. LMC-M WC blend coating - HVOF

The tests focused on elevated-temperature solid-particle erosion under generally oxidizing conditions [32]. The test equipment and procedures have been described in literature [33]. The specific details of the test conditions are given in Table 5-1.

Table 5-1
Test Conditions [32]

Particle velocity	V	141.2 ft/s (40 m/s)
Temperatures	T	900°F (482°C), 1100°F (593°C)
Impact angles	α	30°, 90°
Test time	t	3 hrs.
Loading	L	0.441 Lb_m (0.2 kg)

The results of testing were reported as both a weight loss and thickness loss for each of the tested specimens. However, since the weight measurements included the material erosion wastage (-), oxide scale (+), ash deposition (+), and different densities, the weight loss scheme was not a desirable approach for predicting the erosion rate of specific alloys. This prevents making a comparison between the mathematical models of Finnie and Mamoun [9] (weight loss schemes)

for calculated versus experimental results. Therefore, the thickness loss scheme was the more valid method for determining the erosion rates of the tested alloys.

High-temperature erosion testing was performed on twelve different alloys as previously listed. The alloys were tested at four specific conditions (an explanation is provided beside each permutation).

- 900°F (482°C), 30° impact angle – waterwall environment, ductile-erosion failure
- 1100°F (593°C), 30° impact angle – SH/RH environment, ductile-erosion failure
- 900°F (482°C), 90° impact angle – waterwall environment, brittle-erosion failure
- 1100°F (593°C), 90° impact angle – SH/RH environment, brittle-erosion failure

In boiler service, the ash or soot deposits on the waterwalls and superheat/reheat tubing are stationary, and the sootblower media creates impact. This can be simulated by impacting the given surface with corresponding media and fouling particulate. For example, consider a moving body through a stationary fluid. This can be simulated as a stationary body immersed in a stream of fluid flow. The previous case is used to determine drag experimentally while the testing in this project is synonymous with determining erosion rates of given alloys with soot buildup impacted by sootblowing media.

5.2 Results

Table 5-2 provides the results of high-temperature erosion testing for the twelve materials at four permutations of testing, listed in order of erosion resistance performance. In addition, the graphical results are presented in Figure 5-4, omitting the Duocor coating because its erosion resistance is considerably lower than all other specimens tested, and focusing on those that are of importance for application of erosion resistant overlays/coatings.

Table 5-2
Erosion Wastage Data [32]

No.	Target Material	Thickness loss (μm)			
		At 900°F (482°C)		At 1100°F (593°C)	
		α=30°	α=90°	α =30°	α =90°
1.	Cr_3C_2-NiCr coating	5	19	11	38
2.	WC200 cladding	6	23	13	56
3.	LMC-M+WC coating	20	28	25	99
4.	Inc. 625 weld overlay	54	51	74	90
5.	Inc. 622 weld overlay	56	54	71	104
6.	602CA weld overlay	63	72	75	84
7.	Inc. 52 weld overlay	65	62	68	83
8.	Inc. 72 weld overlay	66	58	73	94
9.	312 SS weld overlay	67	64	70	74
10.	309L weld overlay	71	65	74	85
11.	**SA387 steel**	**76**	**65**	**90**	**97**
12.	Duocor coating	187	752*	226	825*

* Indicates coating worn through

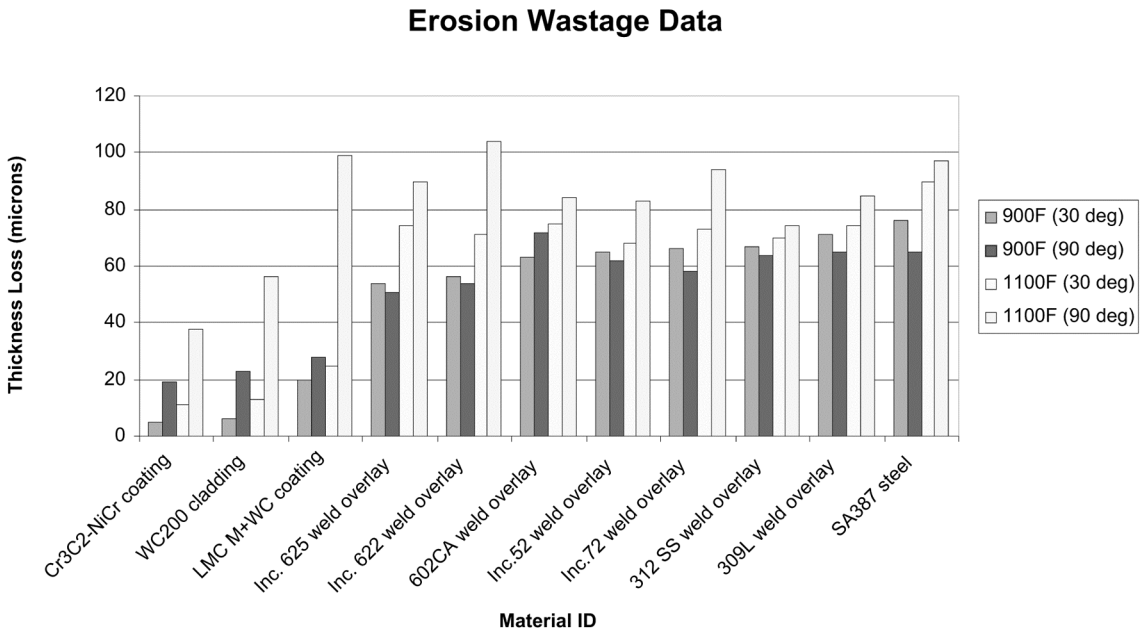

Figure 5-4
Erosion Wastage Data [32]

5.3 Waterwall Tubing Optimum Alloys

To determine the optimal alloy coating for waterwall tubing based upon performance criterion, the data corresponding to the 900°F (482°C) erosion tests will be analyzed (900°F corresponds to about 800°F [427°C] steam temperature for a supercritical boiler). Table 5-2 was simplified by focusing only on the erosion wastage data at 900°F (482°C) to simulate that of waterwall tubes, since waterwalls typically operate in this thermal environment. The Cr_3C_2-NiCr HVOF-applied coating and WC200 infiltration brazed cladding were the most erosion-resistant alloys tested. The LMC-M and tungsten carbide blend applied by HVOF was third. Inconel 625 applied by GMAW performed the best of the nickel alloy subgroup. The stainless steels, SA 387 grade 11 base metal, and Duocor coating followed, respectively in descending erosion-resistance order. The erosion data can be divided into three categories (see Table 5-3) that include:

- Greater than twice the erosion resistance of the base metal
- Similar erosion resistance to the base metal
- High erosion

The Duocor coating was worn through when the angle of impact was 90° (characteristic of brittle-erosion failure). Materials that experienced more thickness loss at lower angles of impact (that is, 30°) exhibit erosion wastage of ductile behavior [34].

Table 5-3
Erosion Performance of Alloys at 900°F (482°C) [32]

		Thickness loss (µm)	
Group No.	**Target Material**	**At 900°F (482°C)**	
		α=30°	**α=90°**
	Cr_3C_2-NiCr coating	5	19
1	WC200 cladding	6	23
	LMC-M+WC coating	20	28
2	Inc. 625 weld overlay	54	51
	Inc. 622 weld overlay	56	54
	Inc.72 weld overlay	66	58
	Inc.52 weld overlay	65	62
	602CA weld overlay	63	72
	312 SS weld overlay	67	64
	309L weld overlay	71	65
	SA387 steel	**76**	**65**
3	Duocor coating	187	752*

* Indicates coating worn through

The following mathematical formulation will be used to approximate the erosion resistance of any given sootblower configuration. The variables involved take into consideration the thickness loss from erosion data at 30° impact (TL_{30}), thickness loss from erosion data at 90° impact (TL_{90}), and the frequency of impact for each (α impacts at 30° per β impacts at 90° exhibited by the given sootblower configuration).

$$SimulatedTL \sim \frac{\alpha(TL_{30}) + \beta(TL_{90})}{\alpha + \beta} \qquad \textbf{Eq. 5-1}$$

5.4 Superheat/Reheat Tubing Optimum Alloys

To determine the optimal alloy coating for superheat/reheat tubing based upon performance criterion, the data corresponding to the 1100°F (593°C) erosion tests will be analyzed. Table 5-2

was simplified by focusing only on the erosion wastage data at 1100°F (593°C) to simulate that of superheat/reheat tubes, since the SH/RH sections typically operate in this thermal environment. When comparing the results to the waterwall tubing optimum alloys section, the Cr_3C_2-NiCr HVOF-applied coating and WC200 infiltration brazed cladding were once again the most erosion-resistant alloys tested. The LMC-M and tungsten carbide blend applied by HVOF was third. Stainless steel 312 and Inconel 52 followed as the best weld overlays. The results show that the stainless steels are more dominant than the nickel alloys at higher temperatures (that is, 1100°F [593°C]), while the opposite is true as was seen in the waterwall tubing optimum alloys section, where the test temperature was 900°F (482°C). The SA387 Grade 11 base metal and Duocor coating follow in descending erosion resistance order, respectively. Once again, the Duocor coating was worn through when the angle of impact was 90° (characteristic of brittle-erosion failure).

Using Equation 5-1, a simulated thickness loss was evaluated for each alloy as shown in Table 5-4. This example uses a long retractable blower with two nozzles opposing each other around the circumference of a lance. Assuming a 2-in. travel per revolution, and a 1-in. shift at the reverse progression, the helical spray pattern of a long retractable blower is shown in Figure 5-5. In the forward progression of a long retractable blower (shown as the solid line in Figure 5-5), a given tube surface will be sprayed at a 90° impact angle; in the reverse progression (shown as the dashed lines in Figure 5-5), the same area will be sprayed twice at lower angles of impact (that is, in the vicinity of 30°, thus α=2 and β=1). As a result, a simulated thickness loss over a three-hour period can be determined for each of the tested materials as shown in Table 5-4.

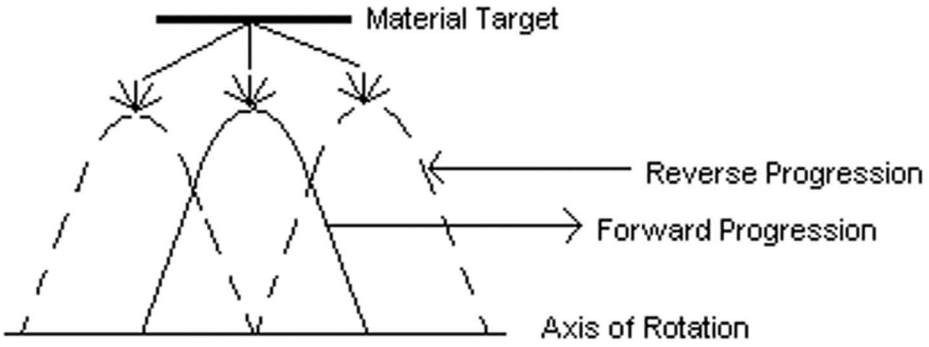

Figure 5-5
Helical Spray Pattern of a Long Retractable Blower

Similar to the waterwall tubing optimal alloys section, erosion data can be divided into three categories (see Table 5-4) with the exception of the LMC-M+WC coating at 90° impact. These three categories include:

- Greater than 1.5 times the erosion resistance of the base metal
- Similar erosion resistance to the base metal
- High erosion

Table 5-4
Erosion Performance of Alloys at 1100°F (593°C) [32]

		Thickness loss (µm)		
Group No.	**Target Material**	**At 1100° F (593° C)**		**Simulated Thickness Loss**
		α=30°	**α=90°**	
1	Cr_3C_2-NiCr coating	11	38	20
	WC200 cladding	13	56	27.3
	LMC-M+WC coating	25	99	49.7
	312 SS weld overlay	70	74	71.3
	Inc.52 weld overlay	68	83	73
	309L weld overlay	74	85	77.7
2	602CA weld overlay	75	84	78
	Inc. 625 weld overlay	74	90	79.3
	Inc.72 weld overlay	73	94	80
	Inc. 622 weld overlay	71	104	82
	SA387 steel**	**90**	**97**	**92.3**
3	Duocor coating	226	825*	425.7

* Indicates coating worn through
** Base metal

5.5 Summary

The results indicate that through all permutations of testing, among the twelve alloys tested, the Cr_3C_2-NiCr HVOF-applied coating showed the highest erosion resistance. In sequence, the second was the infiltration brazed WC200 cladding, and the third was the HVOF LMC-M WC blend coating. The Duocor TWAS-applied coating showed much higher wastage than the SA387 Grade 11 base metal. All weld overlays exhibited similar erosion resistance as that of the base steel, only slightly reduced erosion wastage at a 30° impact angle.

It is apparent from Table 5-2 and Figure 5-4 that all coatings tested at 1100°F (593°C) showed brittle material erosion behavior as demonstrated by the higher erosion wastage at a steep angle than that at a shallow angle. On the other hand, examining testing at 900°F (482°C), the thickness loss of the base metal and all weld overlays were primarily dominated at the 30°

impact angle, characteristic of ductile material erosion behavior. During testing at the higher temperature, it was thought that an oxide scale developed on the surface of steel or overlay alloys, which could prevent the impacting particles from plastically deforming the ductile base metal beneath it [32]. The application process was important in both determining the erosion resistance of a given alloy and developing the bond strength between the coating and base metal.

6
REPAIR METHODS

The following section will illustrate the two main repair categories for sootblower erosion-resistant alloy applications: weld overlays and thermal-spray coatings. The following are the most commonly utilized welding methods for tube overlays:

- Gas metal arc welding (GMAW or MIG)
- Gas tungsten arc welding (GTAW or TIG)
- Plasma arc welding (PAW)
- Shielded metal arc welding (SMAW)

There are also subcategories for thermal-spray coatings that include:

- High-velocity oxy-fuel (HVOF)
- Detonation gun (D-Gun)
- Plasma spray
- Twin wire arc spray (TWAS)

Illustrations and basic characteristics of each of the above methods will be given. Also, comparisons will be made between welding and thermal-spray applications. Application methods are just as important as the alloy selection itself. Optimal repair will focus equally on both the alloy selection and application method.

6.1 Welding

The process of surfacing by welding is commonly referred to as hard facing, cladding, and overlaying [3]. It is characterized by exhibiting thick deposit layers through melting coating alloys on the component surface by gas or arc welding. The coating material can be applied in the form of powder, paste, rod, strip, or wire. The choice of optimum overlay coating alloys is dependent upon the oxidizing, corrosive, and erosion-wear environmental conditions. The following application methods will be discussed: gas metal arc welding (GMAW), gas tungsten arc welding (GTAW), plasma arc welding (PAW), and shielded metal arc welding (SMAW).

Table 6-1 provides an example of a list of materials for bulk coating in high-temperature applications and the typical deposition methods.

Table 6-1
Materials for Bulk Coating in High-Temperature Applications [3]

Classification		Deposited Hardness (kg/mm^2)	Deposition Method*						Temp. Limit °F (°C)
Group	Type		OA	MMA	MIG	FCA	TIG	SA	
Steel	Martensitic Cr	350–650		X	X	X		X	1026 (552)
Steel	High speed	600–700		X	X			X	1116 (602)
Steel	Austenitic stainless	200–500		X			X		1206 (652)
Steel	Austenitic Cr Mn	200–600		X		X		X	1116 (602)
Iron	Austenitic	300–600		X		X			936 (502)
Iron	High Cr austenitic	500–750	X	X	X	X	X	X	1026 (552)
Iron	High Cr martensitic	500–750	X	X	X	X		X	1026 (552)
Iron	High Cr complex	600–800		X	X	X		X	1296 (702)
Nickel alloy	Ni Cu	130		X					936 (502)
Nickel alloy	Ni Mo Cr W	250–500	X	X	X		X		>1476 (802)
Nickel alloy	Ni Cr B	200–750	X	X			X		>1476 (802)
Nickel alloy	Ni Cr Fe	120–200		X	X		X	X	>1476 (802)
Nickel alloy	Ni Mo Fe	200–300		X					>1476 (802)
Cobalt alloy	Co Cr W low alloy	350–400	X	X	X		X	X	>1476 (802)
Cobalt alloy	Co Cr W med alloy	400–500	X	X	X		X	X	>1476 (802)
Cobalt alloy	Co Cr W high alloy	500–650	X	X	X		X	X	>1476 (802)
Cobalt alloy	Co Cr W Ni alloy	-	X	X	X		X		>1476 (802)

* OA = Oxyacetylene; MMA = Manual Metal Arc; MIG = Metal Inert Gas; FCA = Flux-Cored Arc; TIG = Tungsten Inert Gas; SA = Submerged Arc

6.1.1 Gas Metal Arc Welding (GMAW)

GMAW or MIG is an electrical arc welding process in which an arc is struck between a consumable wire electrode and the workpiece [35]. Shielding is provided by an inert gas; therefore, MIG refers to metal inert gas. The following characteristics are those of the GMAW process as illustrated in Figure 6-1:

- Uses a consumable wire electrode
- Uses shielding gas
- Results in a uniform and slag-free weld bead
- Is commonly used for automated welding

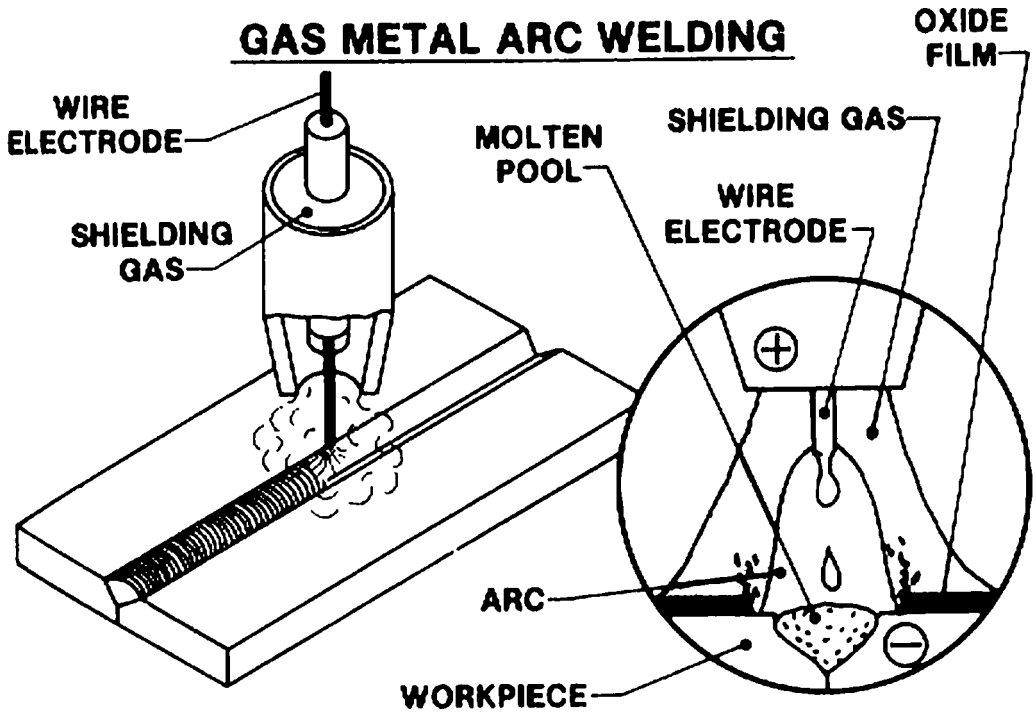

Figure 6-1
Gas Metal Arc Welding [35]

6.1.2 Gas Tungsten Arc Welding (GTAW)

GTAW or TIG is an electrical arc welding process in which an arc is struck between a nonconsumable tungsten electrode and the workpiece [35]. Gas shielding is provided to protect the molten metal from contamination; therefore, TIG refers to tungsten inert gas. Constant

amperage is applied during this welding process. The following characteristics are those of the GTAW process as illustrated in Figure 6-2:

- Uses a nonconsumable tungsten electrode
- Uses shielding gases (Ar, He, or CO_2)
- Produces very high-quality welds with no slag or spatter
- Is readily applied to thin materials

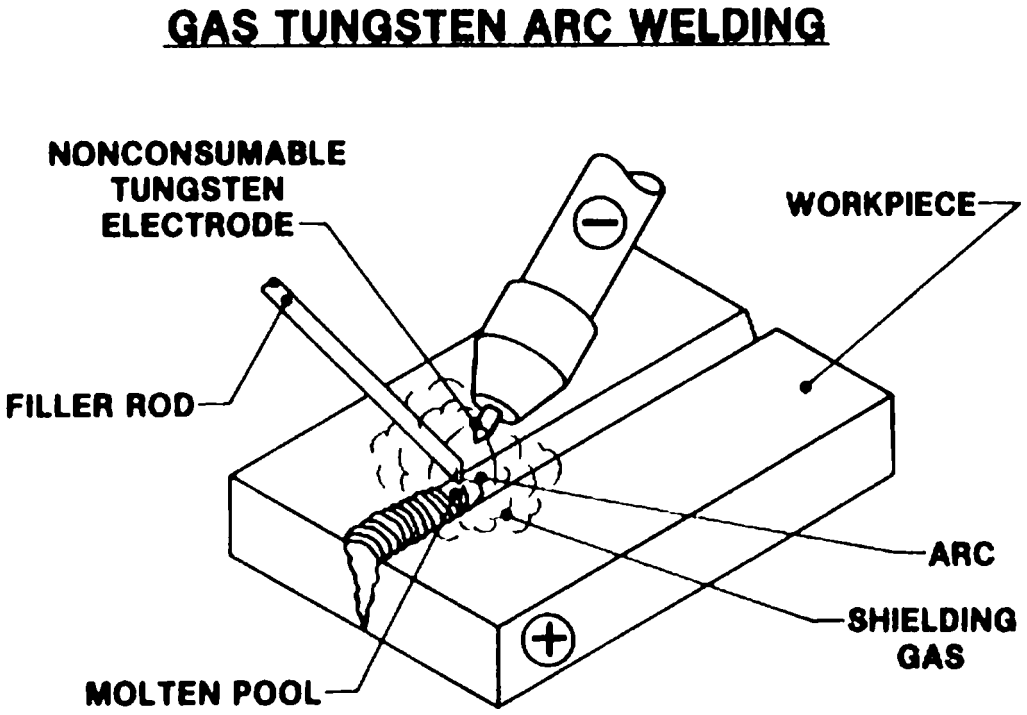

Figure 6-2
Gas Tungsten Arc Welding [35]

6.1.3 Plasma Arc Welding (PAW)

In PAW a shielded arc is struck between a nonconsumable electrode and the torch body, and the arc transforms an inert gas into plasma [35]. This plasma is then used to melt the workpiece and filler metal. The following characteristics are those of the PAW process as illustrated in Figure 6-3:

- Uses a nonconsumable tungsten electrode
- Requires shielding gases (Argon, Helium, and Nitrogen) to form the plasma
- Produces a high-temperature arc of 30,000ºF (16,649ºC)

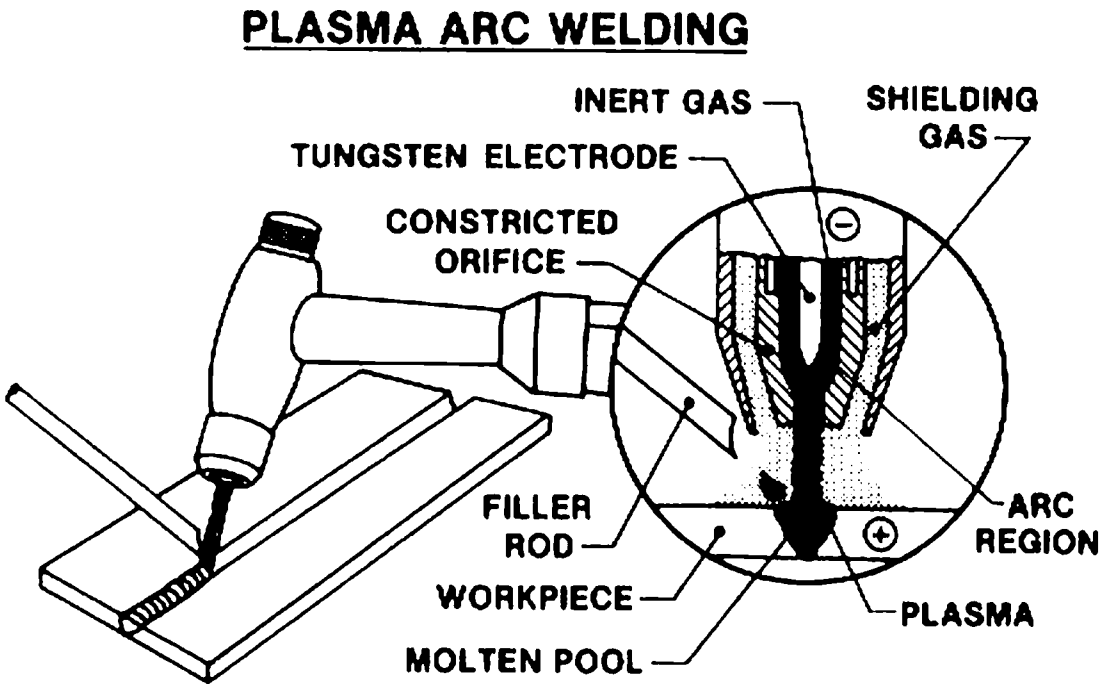

Figure 6-3
Plasma Arc Welding [35]

6.1.4 Shielded Metal Arc Welding (SMAW)

In SMAW an electric arc is established between a flux-coated consumable rod electrode and the workpiece [35]. A gas shield is formed by the vaporization of the flux coating. The following characteristics are those of the SMAW process as illustrated in Figure 6-4:

- Uses a consumable rod electrode
- Deposits slag on the weld bead
- Provides shielding by vaporization of the flux coating on the electrode
- Supplies constant welding current
- Depends on operator skill in maintaining a constant arc length and travel speed for quality and appearance of weld

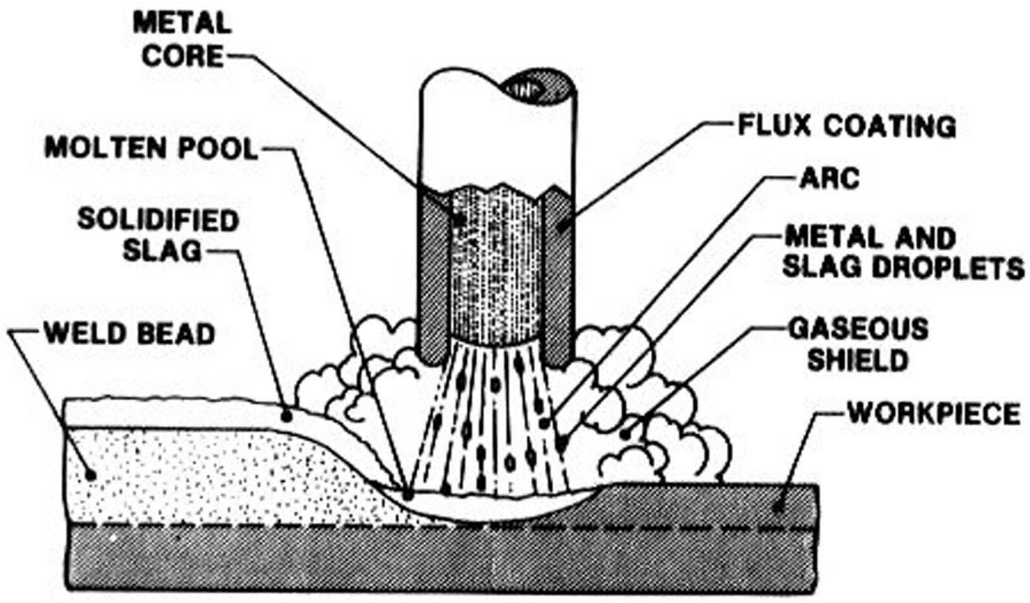

Figure 6-4
Shielded Metal Arc Welding [35]

6.2 Thermal Spray

Thermal-spray coatings are usually comparatively thin, usually less than 19.7 mils (0.5 mm) [2]. These coatings create a barrier layer for protecting the underlying metal from wastage, thus requiring exceptional corrosion and wear-resistant properties in high-temperature applications. In some situations this form of protection is inadequate, as the thin coatings have limited life expectancy in hostile environments. However, current technology has produced coatings that work exceptionally well in preventing tube wastage. The following application methods are discussed: high-velocity oxy-fuel (HVOF), detonation gun (D-Gun), plasma spray, and twin wire arc spray (TWAS).

The first step is always to prepare the surface for application of the coating [36]. This should be performed by cleaning and then by roughening using a process that will not contaminate it with oil or other objectionable substances. One of the most widely used preparation processes is grit blasting by rough mesh sand or aluminum oxide (or other proprietary products). Other practices that are acceptable include rough turning, or threading and knurling.

6.2.1 High-Velocity Oxy-Fuel (HVOF)

The HVOF thermal-spray process is characterized by accelerating the coating particles to supersonic speed, which achieves a remarkably high degree of bond strength at the substrate interface and a very limited level of porosity [36]. The process is essentially a continuous one; depending on the parts to be coated, they may end up hotter than by application with other spray processes. Therefore, special provisions may be required to prevent overheating. The equipment is similar to the plasma spray gun with the required modifications needed to sustain higher

temperatures and gas speed. It was developed in the search for better properties of the deposited layers at a time when the D-Gun was proprietary and enjoyed a monopolistic market position. HVOF systems are field portable, but are primarily used in fabrication shops.

6.2.2 Detonation Gun (D-Gun)

The Detonation Gun (D-Gun) is a piece of thermal-spray equipment developed to produce superior coating properties [36]. It is a water-cooled barrel where oxygen, fuel (mostly acetylene), and powder are admitted through valve-controlled ports, and where the explosive mixture is ignited by a spark at every cycle to propel the heated particles of the powder at supersonic speed upon the substrate to be coated, located at a certain distance from its mouth. Cycles are repeated with a frequency of a few tenths of a second. The succession of explosions performing the coating work produces an elevated level of noise, which must be controlled by locating the equipment in properly insulated facilities. Detonation flame spraying can only be performed in a fabrication shop.

6.2.3 Plasma Spray

This thermal-spray process has higher bond properties of the sprayed layers and lower porosity and internal defects than any other thermal-spray process discussed [36]. The process is described by a very hot gas in a highly ionized form (which is one deprived of some of its electrons by the passage through a powerful electric arc). A special torch or gun is designed to generate the plasma flame by passing high-pressure gas through a constricted or confined arc between water-cooled nonconsumable electrodes, a cathode, and a hollow anode nozzle. The plasma flame meets and carries along the powder fed through the side of the nozzle and heats the particles to a very high temperature to a molten or plastic state. It then propels them with high velocity toward the surface to metallize. The gases used for making the plasma are normally nitrogen mixed with about 10% hydrogen.

In order for proper and continuous thermal-spray operation, all of the main parameters must be constantly controlled and adjusted by automatic provisions once the flame temperature has been selected by changing the ratio of electric current to plasma gas [36]. With a special arrangement, one can spray a buffer layer with one material and then move gradually to a different material so that the proportions of the two change continuously along the thickness of the sprayed overlay. Such a development has very useful and interesting applications. In modern setups, all of the functions are computer-controlled. A robot holding the plasma gun against the work piece fastened to a rotating positioner is instructed to provide the plasma layers where needed, in the most accurate and repeatable process. Plasma spray can be applied in air or in a vacuum chamber (in this case some of the properties are improved). Plasma spray is primarily performed in fabrication shops.

6.2.4 Twin Wire Arc Spray (TWAS)

This thermal-spray process is performed with a special torch that feeds two electrode wires, with opposite electrical charges, meeting at their tips where an arc is struck between them [36]. The electrode metal is atomized and sprayed by the propelling gas, usually compressed air, onto the

substrate. This process has been used for spraying aluminum or zinc on steel structures to protect them in marine environments. For best performance, the coating is usually sealed with organic compounds. This thermal-spray process was a development that had some popularity when it first appeared, but in recent times has largely been replaced by more modern and effective processes. Traditionally, electric arc guns have been too bulky and cumbersome for fieldwork.

6.3 Welding Versus Thermal Spray

Boiler tube walls are subjected to high-velocity gas flow with entrapped solid particulate matter. Many techniques have been proposed to reduce tube wear. At the moment, the simplest approach consists of shot blasting the walls to produce a mechanically adherent surface, followed by metal spraying [37]. Various spray-coating materials are currently in use. If for some reason a small section of the sprayed coating becomes detached, as is known to happen, preferential wear occurs at that position, and maintenance interventions such as cutting and replacing boiler tube sections become necessary.

Many of the thermal-spray methods explained earlier have been tried for protection from waterwall corrosion and sootblower erosion protection with mixed results. None of the coatings form a metallurgical bond, but the denser coatings seem to perform better than the less-dense processes like TWAC. Propriety coating methods are continually being developed and offer higher impact velocities that provide higher bond strength and a denser coating.

To be successful, a sprayed coating when applied to a base metal as convoluted as a waterwall requires the following [37]:

- An absolutely clean base metal, mechanically roughened by an angular shotblasting media, and perfectly free of pre-existing debris and complex coating
- Spraying applied normally to the surface
- A base metal not subject to large temperature fluctuations and preferably exhibiting similar thermal properties to the coating
- A substrate that will not be subject to mechanical strains (such as occurs on sections of the waterwall during heating)
- No areas presenting substantial porosity

These conditions are not compatible within a boiler enclosure and especially not with tube walls that were subjected to previous repairs and renewals [37]. Spray coatings have been shown to be exceptionally wear-and-corrosion-resistant when applied under ideal conditions imposed during laboratory testing, but not under conditions during a boiler repair campaign. Reliability of a sprayed-on coating is generally only acceptable as cladding in areas where simple erosion needs to be checked. These restrictions do not exist with welded coatings.

Cladding the area by welding ensures that the surface is completely protected and no failure occurs as previously mentioned. This produces the necessary reliability not previously available, but generally at a higher cost, while requiring a longer outage duration to perform the welding overlay.

Typical waterwall tubing material is usually produced from carbon or low-alloy steel up to and including T11 (1 ¼ CR ½ Mo). Some high-temperature waterwalls in supercritical power plants even contain T22 (2 ¼ Cr 1 Mo) or newer advanced ferritic alloys such as T23 [37]. Steel tubing with a simultaneously extruded 304 stainless skin has been used in some SH/RH applications. These higher alloy materials have higher hardenability, which is a concern for overlay applications. It is now generally accepted that weld overlays can be performed on carbon steel tubes and low-alloy tubing up to and including materials classified as P4 by the ASME Code (1 ¼ Cr ½ Mo) without preheat or postweld heat treatment (PWHT). Higher alloy materials generally require higher preheat and PWHT.

Successful cladding of waterwalls is characterized by significantly low porosity, a reasonably smooth surface, and adequate erosion and corrosion resistance [37]. Reduction of residual stresses can be achieved through use of water backing during the welding process. The deposit must exhibit no significant spatter, negligible undercut, a low dilution level, and be free of lack-of-fusion defects and cold-lapping zones.

Repair and cladding of waterwalls can take place when the tubes are either full or empty of water [37]. Water backing is recommended to allow for faster travel and a more consistent process while reducing distortion and residual stresses. Although new tube thicknesses are generally greater than 0.197 inches (5 mm), after abraded they may be much thinner. However, a minimum wall thickness of 0.100 inches (2.54 mm) is recommended for cladding. These circumstances require water-filled tubing that is essential to prevent burn-through of the wall. Table 6-2 provides general welding parameters for different products.

Table 6-2
Laboratory Results for Welding of Various Products and Variables [37]

Product	Water		Wall (mm/in.)		Amp I	Volt V[a]	Osc. (mm/in.)	Freq. N/min	Speed cm/ft per min	Dep. kg/hr	Dilution %[b]
	On	Off	5/ 0.2	3/ 0.12							
TubeS[c] 309Mo	*		*		160	22	12/0.47	50	30/0.98	1.8	18
"		*	*		120	20	11/0.43	45	20/0.66	1.4	20
"	*			*	130	21	11/0.43	50	20/0.66	1.5	20
"		*		*	100	19	10/0.39	40	16/0.53	1.0	20
Steltube[c] 625	*		*		160	22	12/0.47	50	30/0.98	1.8	N/A
"		*		*	120	20	11/0.43	50	18/0.59	1.4	N/A
"		*		*	100	19	10/0.39	40	15/0.49	1.0	N/A
Stelloy 625	*		*		170	24	12/0.47	40	20/0.66	1.5	25
"		*	*		140	22	10/0.39	40	16/0.53	1.2	22
"	*			*	140	22	10/0.39	40	16/0.53	1.2	30
"		*		*	No suitable conditions found.						

Notes: kg/hr is wire consumed.

(a) Average voltage - power supply used was pulsed.

(b) Obtained by analysis of the deposited metal.

(c) Specially formulated for positional work. Laboratory results obtained from cladding single lengths of 1.97-in.-(50-mm-) diameter mild steel tubing. Welding wire 0.047 in. (1.2 mm) tubular Tube-S[c] 309Mo(1)-G, Steltube[c] 625-G and solid Stelloy 625-G all welded with Argon + 2% O_2.

For further information regarding solid welding wire as opposed to tubular flux-cored, welding equipment, case history and observations, cladding time and cost, and material comparison, refer to "In Situ Weld Cladding of Abraded Boiler Tube Walls: Materials and Programmable Portable Equipment" in EPRI's *Welding and Repair Technology for Power Plants* [37].

7
CONCLUSIONS

Boiler tubes begin to develop fireside fouling as a result of the combustion of coal. This fouling creates an additional layer of material with low thermal conductivity. Thus, the efficiency of the boiler diminishes over time. Sootblowers are used to remove this undesired layer and restore the boiler to optimal conditions. However, sootblowing too often removes the protective oxide layer on tube surfaces, making them more susceptible to corrosion or erosion-corrosion damage.

This document provides relevant background information on topics such as sootblowers, cleaning media, and common damage mechanisms. A more technical discussion, both from an experimental and theoretical perspective, is provided on subjects such as erosion testing, mathematical erosion models, and high-temperature material wear. A list of twelve alloys was developed, including a brief summary, specifications, chemical composition, thermal data, application method, and cost estimate for each. The alloys were tested at four conditions: 900°F (482°C) 30° impact angle, 900°F (482°C) 90° impact angle, 1100°F (593°C) 30° impact angle, and 1100°F (593°C) 90° impact angle. A mathematical erosion model was formulated to derive a simulated thickness loss for any sootblower configuration. An example in the superheat/reheat tubing section of a boiler unit is provided using a specific sootblower configuration to determine optimum alloys for repair of superheat/reheat tubes. Several repair methods are discussed, including welding techniques and thermal-spray application methods.

The results show that the Cr_3C_2-NiCr, W200, and LMC-M coatings consistently outperformed all other alloys in high-temperature erosion resistance. However, erosion performance is not the only criterion used in selecting an appropriate alloy for waterwall or superheat/reheat tubing environments. Moreover, other issues to be evaluated deal with cost, boiler environment, ease of application, and sootblower configuration. For an application example, the WC200 infiltration-brazed cladding can be used only as new tube replacements or applied as a custom-fabricated wear liner, while other applications can be used in service without tube bank removal or custom fabrication. The results from high-temperature erosion testing are provided to allow the user some insight as to what alloys may be optimum for specific boiler environments—this is by no means a definite listing of what alloys should be chosen.

Additionally, welding vendors and utilities using 309, 625, and 622 welding overlays for repair of eroded areas have reported good results [38].

8
REFERENCES

1. *Annual Book of ASTM Standards,* V*ol. 03.02, Wear and Erosion: Metal Corrosion.* American Society for Testing and Materials, Philadelphia, PA, 1991.

2. *Guidelines for Intelligent Sootblowing Control.* EPRI, Palo, Alto, CA: 2000. 1000410.

3. *Erosion Wear in Coal Utilization*. Hemisphere Publishing Corporation, New York, NY, 1998.

4. *Steam: Its Generation and Use,* 40th Edition. S. Stultz and J. Kitt, eds. Babcock & Wilcox, Co., Barberton, OH, 1992.

5. *Fourth Intelligent Sootblowing Workshop Proceedings*. EPRI, Palo Alto, CA: 2002. 1004112.

6. *Metals Handbook*. H. Boyer and T. Gall, eds. American Society for Metals, Metals Park, OH, 1992.

7. *Boiler Tube Failures: Theory and Practice, Vol. 2, Water Touched Tubes.* EPRI, Palo Alto, CA: 1996. TR-105261-V2.

8. http://dnclab.berkeley.edu/~mschmit/html/E190_Final.pdf, July 9, 2003.

9. *Erosion-Corrosion of Metals and Alloys at High Temperatures.* EPRI, Palo Alto, CA: 1984. CS-3504.

10. *Water Blowing of Fireside Deposits in Coal-Fired Utility Boilers*. EPRI, Palo Alto, CA: 1997. CS-4914.

11. http://www.corrosionsource.com/events/intercorr/techsess/asm/asm2.htm, March 17, 2003.

12. *Corrosion and Particle Erosion at High Temperatures*. V. Srinivasan and K. Vedula, eds. The Minerals, Metals, and Materials Society, Las Vegas, NV, 1989.

13. Y. Nishiyama, Y. Hayase, and N. Otsuka, *Corrosion-Resistant Boiler Tube Materials For Advanced Coal-Fired Steam Generating Systems.* Sumitomo Metal Industries, Ltd.

14. *Super Hard Steel Elevated Temperature Erosion Test Data Sheet*, SHS-717. NanoSteel Company, 2003.

15. http://www.powerspray.com/hitemp.html, March 17, 2003.

16. W. Seitz, *FWESI Thermal Spray Services Waterwall Corrosion Project Coating and Overlay Performance Assessment*. Foster Wheeler Development Corporation, FWDC No. 9-25246800, April 1, 1998.

17. *Liquidmetal Coatings Brochure,* 2003.

18. *ASME Boiler and Pressure Vessel Code, Section II, Part A, Ferrous Material Specifications.* American Society of Mechanical Engineers, New York, 1995.

19. http://www.xergon.com/catalog/ch9ref.pdf, October 3, 2003.

20. http://www.specialmetalswelding.com, September 17, 2003.

21. *ASME Boiler and Pressure Vessel Code, Section II, Part C, Specifications for Welding Rods, Electrodes, and Filler Metals*. American Society of Mechanical Engineers, New York, 2001.

22. http://www.matweb.com, October 3, 2003.

23. S. Kiser, Special Metals Welding Products Company, Consulting (September 18, 2003).

24. http://www.brazing.com, September 24, 2003.

25. http://www.techalloy.com/highnickelweldingwires.htm, October 3, 2003.

26. *The world of ThyssenKrupp.* VDM Edition, CD-ROM, 2002.

27. http://www.amfiller.com/products/2218, September 22, 2003.

28. http://www.conformaclad.com, May 20, 2003.

29. Z. R. Shui, Buqian Wang, Consulting (November 23, 2003).

30. *Duocor Liquidmetal Technologies Material Safety Data Sheet,* January 2001.

31. L. Robbins, Liquidmetal Coatings, Personal Communication (August 2003).

32. B. Wang, *A Comparison of Erosion Resistance of Twelve Different Materials.* Technical and Research Memorandum, Nov. 13, 2003. LBW001-1.

33. V. Levy and Y. F. Man, "Erosion-Corrosion of Chromium Steel." *Corrosion-Erosion-Wear of Materials at Elevated Temperatures.* NACE, 1986.

34. M. Hutchings. *I.M. Tribology: Friction and Wear of Engineering Materials.* CRC Press, Boca Raton, FL, 1992, p.133–197.

35. http://class.et.byu.edu/mfg130/processes/thermaljoining.htm, July 29, 2003.

36. http://www.welding-advisors.com/Thermal-spray.html, July 29, 2003.

37. D. W. Gandy and S. J. Findlan, *Welding and Repair Technology for Power Plants*, Second International Conference. EPRI Proceedings (1997). TR-107719.

38. WSI and Selected Utilities, Personal communication.

Program:
Fossil Materials and Repair

About EPRI

EPRI creates science and technology solutions for the global energy and energy services industry. U.S. electric utilities established the Electric Power Research Institute in 1973 as a nonprofit research consortium for the benefit of utility members, their customers, and society. Now known simply as EPRI, the company provides a wide range of innovative products and services to more than 1000 energy-related organizations in 40 countries. EPRI's multidisciplinary team of scientists and engineers draws on a worldwide network of technical and business expertise to help solve today's toughest energy and environmental problems.

EPRI. Electrify the World

Printed on recycled paper in the United States of America

1008037

EPRI • 3412 Hillview Avenue, Palo Alto, California 94304 • PO Box 10412, Palo Alto, California 94303 • USA
800.313.3774 • 650.855.2121 • askepri@epri.com • www.epri.com